Egyptian Journal of Chemistry

http://ejchem.journals.ekb.eg/

Synthesis, Molecular Docking, DFT and Pharmacophore Studies of New Naphthalene-Heterocycle Hybrids of Prospective Antiviral Activity

Mohamed A. Elsayed[a]*, Ashraf M. Mohamed[a]*, Salwa F. Mohamed[a], Dina H. Elnaggar[a], Naglaa A. Abdel-Hafez[a], Mohamed GabAllah[b], Eman S. Abou-Amra[c] and Ahmed M. Hussein[d].

[a]*Applied Organic Chemistry Department, National Research Centre, Dokki 12622, Cairo, Egypt.*
[b]*Center of Scientific Excellence for Influenza Viruses, National Research Centre, El-Buhouth Street, Dokki, Cairo, 12622, Egypt*
[c]*Organic Chemistry Department, Faculty of Science, Al-Azhar University (Girls) Nasr City, 11751, Egypt.*
[d]*Chemistry Department, Faculty of Science, Beni-Suef University, Beni-Suef 62511, Egypt.*

Abstract

The rate of anti-viral drugs resistance has increased dramatically even while there are fewer new antivirals available agents. The COVID-19 pandemic has highlighted the necessity of further endeavors to create comprehensive treatments to counteract SARS-CoV-2 infection. In the current study, an attempt to synthesize numerous *N*-heterocycles of substituted pyridine and pyrazole constituents have a marked family of molecules with a significant function in medicinal chemistry as promising possibilities for future antiviral drugs. Enaminones play a crucial role in the synthesis of diverse nitrogen-containing heterocyclic compounds. Heterocyclization of enaminone **2** with 6-amino-2-thioxopyrimidine-4-one **(3)** afforded the corresponding 2-thioxopyrido[2,3-d] pyrimidine-4-one derivative **5**. Some new 1-aryl-3,4-disubstituted pyrazoles **8a-e** were synthesized via the reaction of hydrazonoyl chloride derivatives **7a-e** with enaminone **2**. Pyrazolo[3,4-d] pyridazine derivative **9** was obtained through the hydrazinolysis of the new 1-aryl-3,4-disubstituted pyrazole derivative **8e.** As well, malononitrile and 2,4-pentandione reacted with enaminone **2** to afford 6-naphthyl-2,3-disubstituted pyridines **10** and **11**, respectively. Novel two pharmacophoric models of substituted [1,2,4]triazolo[1,5-a]pyrimidine **12** and [4,5]imidazolo[1,2-a]pyrimidine **13** were synthesized in good yield. Microanalytical data and elemental analysis have been used to prove the chemical structures of the new products. The antiviral activity of the new synthesized compounds was tested against VERO-E6 cell lines and compounds **8a**, **8b** and **8d** exhibited good inhibition activities against SARS-COV 2 virus with selectivity index (SI) 21.98 and 27.73, respectively. Docking investigation of the designed structures has been studied into SARS-CoV-2 spike glycoprotein (PDB ID: 6VSB) and compounds **8b** and **8d** showed good fitting inside the binding site of the protein molecular surface with minimum binding energy. Additionally, we used density-functional theory (DFT) to examine the molecular geometry and structure of the more effective compounds to deduce their antiviral effects.

Keywords: Enaminone, triazolopyrimidine, imidazolepyrimidine, pyrimidine-4-one, pyrazolopyridazine, hydrazonyl chloride, docking, antiviral.

1. Introduction

SARS-CoV-2, the virus that causes severe acute respiratory syndrome coronavirus 2, belongs to a large family of viruses called coronaviruses. Both humans and definite animals are apt to infection by these viruses. The COVID-19 pandemic, which is characterized by a high rate of spread, has affected every aspect of the community. It has presented a significant challenges to both healthcare and frugality. In 2019, the first proven case of SARS-CoV-2 infection in people was checked [1]. It is believed that, droplets liberated when an infective person coughs, sneezes or speaks can transmit the virus to another person at a high rate [2]. It can also be transferred by touching one's mouth, nose or eyes after coming into contact with a surface that has been infected but this way is less common. Many organ fiasco and severe acute respiratory disease are prospective consequences of SARS coronavirus infections. Zou and his team work identified in their investigation the organs like the heart, lung, kidney, esophagus, ileum, and bladder, and located specific cell types, at venture and susceptible to CoV-19 infection [3]. The pathogenesis of SARS-CoV-2 states that the virus propagates firstly in the upper respiratory tract mucosal epithelium and then reduplicates further in the lower respiratory tract and gastrointestinal mucosa [4]. Research is being conducted to treat COVID-19 and stop SARS-CoV-2 infections. Consequently, we devoted our efforts to synthesize some new naphthalene-heterocycle hybrids and investigate their antiviral activity.

*Corresponding author e-mail: ammewas1@gmail.com.; (Ashraf M. Mohamed).
Received date 19 October 2024; Revised date 19 March 2025; Accepted date 19 March 2025
DOI: 10.21608/ejchem.2025.329489.10655
©2025 National Information and Documentation Center (NIDOC)

Enaminones acquired great fame in organic chemistry research in recent years. Moreover, they are one of the most attractive building blocks for the synthesis of several new biologically active nitrogen-containing heterocyclic compounds such as pyridines and pyrazoles [5, 6]. In the current investigation, enaminone has been established as a starting material for the synthesis of different nitrogen-containing heterocycles *via* its condensation with 2-acetyl naphthalene. In medicinal chemistry, naphthalene comprises many-sided and multipurpose podiums [7]. This nucleus indicates an auspicious core in medication designing due to its various biological efficiencies resulting from structural modulations. The broad spectrum of naphthalene in pharmacological applications such as anticancer [8], antimicrobial [9], anti-inflammatory [10], antiviral [11], antitubercular [12], antihypertensive [13], antidiabetic [14], anti-neurodegenerative [15], antipsychotic [16], anticonvulsant [17] and antidepressant [18], make it a fertilizing subject for research study. Besides, different naturally occurring compounds including the naphthalene nucleus revealed highly significant biological activities such as bis-ANS 82, Rifampicin, Justiprocumin A, B, Patentiflorin A, and podophyllotoxins (Etoposide, Teniposide). Nitrogen-containing scaffolds pendent to naphthalene core demonstrate strong antiviral and cytotoxic action against different viral cell lines [19, 20]. They have the potential to affect various stages of the viral life period at several points, including the virus's entry into host cells, the emergence of novel viral genders, and the virus's genome replication. In order to achieve duple-drug efficacy, hybrid compounds such as Naphyrone, Tolnaftate and Naftifine combine two or more different biologically efficient moieties into one structure [21] **(Figure 1)**. Drug hybridization can prevent popular dual-drug reactions seen in drug mixing and produce novel molecules with low toxicity, better similarity, and best pharmacokinetics.

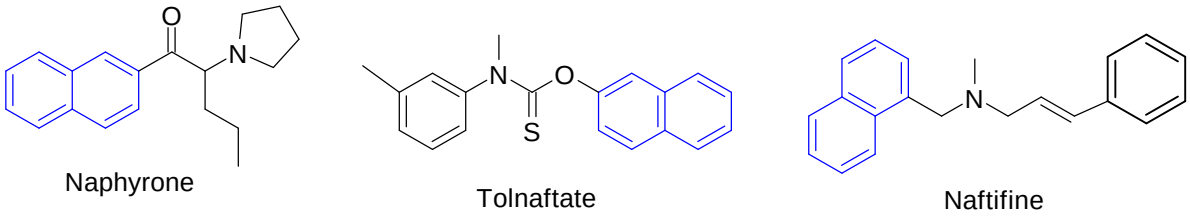

Fig. 1. Drugs containing naphthalene structure.

According to these findings and continuation of previous work [22-26], we planned our investigation to synthesize a range of nitrogen containing heterocyclic compounds that hybrid with naphthalene scaffold and examined their viral effects against various cell lines. Additionally, one of the most important calculations to optimize the molecular structure of the prepared compounds is density functional theory (DFT) methods, which are commonly employed for the assessment of several molecular characteristics. Research was conducted using frontier molecular orbitals (FMOs) to shed light on charge transfer [27] in the molecules under test. Moreover, the study involved HOMO and LUMO analysis. Using molecular electrostatic potential (MEP) analysis, the electron distribution, active nucleophilic and electrophilic sites of the selected compounds were determined. Also, to understand how the tested compounds attach to their target protein and exert their antiviral action and also to understanding the binding mechanism, binding affinity and non-bonding interactions, molecular docking experiments were conducted against the SARS-CoV-2 spike glycoprotein (PDB ID: 6VSB). Lastly, a hypothetical pharmacophore model was constructed utilizing the Molecular Operating Environment (MOE) tool using nine compounds with proven antiviral activity. In conclusion, the computation of the pharmacophoric model and the antiviral activity of the more active drugs were both topics of considerable interest in the study.

2. Results and Discussion

2. 1. Chemistry

The chemistry of Enaminones has received great attention as readily obtainable building blocks possessing multi-electrophilic and nucleophilic moieties [23]. One of the most important methods for preparation of enaminone is the condensation of active methylene compounds with formamide acetals. Therefore, 3-(dimethylamino)-1-(naphthalene-2-yl)prop-2-en-1-one (**2)** was generated by condensation of dimethyl formamide-dimethyl acetal (DMF-DMA) in dry *p*-xylene with 2-acetyl naphthalene **1** under reflux for 35h produced **2** in 75% yield as yellow crystals [22,27] (**Scheme 1**).

The stereochemistry for the structure of enaminone **2** was identified as *E*-isomer [5, 6, 22, 23]. The ^{1}H NMR spectrum of enaminone **2** displayed two doublet signals at δ 5.98 and 7.75 ppm with *J*-coupling constant 12 Hz for two olefinic protons and two singlet signals at δ 2.96 and 3.15 ppm for $N(CH_3)_2$. The mechanism of formation of enaminone **2** was illustrated in scheme 1. An addition-elimination reaction mechanism occurs to remove two molecules of MeOH and the enaminone compound **2** is formed

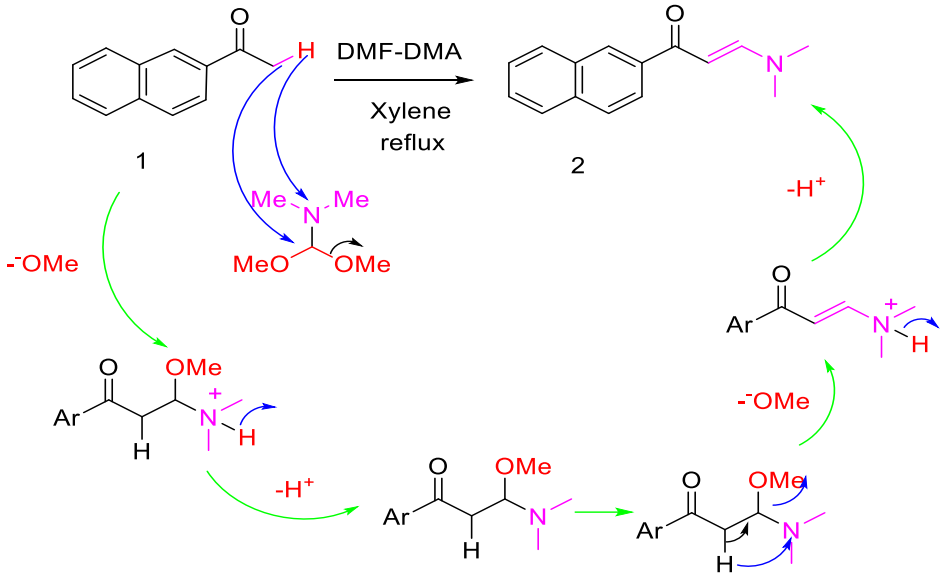

Scheme 1: Mechanism for synthesis of enaminone 2

Naphthalene-thiopyrimidine hybrid was obtained from refluxing enaminone **2** with 6-amino-2 thioxopyrimidin-4-one **3** in the presence of glacial acetic acid, to afford the corresponding conjugate 2-thioxopyrido[2,3-*d*]pyrimidine-4(1*H*)-one derivative **5** rather than its isomeric one **6**. Compound **5** was confirmed chemically, when refluxing 6-amino-2-thioxopyrimidin-4-one **3** with DMF-DMA to give *N*,*N*-dimethyl-*N'*-(6-oxo-2-thioxo-1,2,3,6-tetrahydropyrimidin-4-yl) formimidamide **4** [22], which was reacted with 2-acetylnaphthalene in boiling glacial acetic acid to afford compound **5** (Scheme 2). Additionally, the IR spectrum of compound **5** showed absorption bands at 3154, 3054 and 1687 cm^{-1} attributed to 2NH and carbonyl groups respectively. The ^{1}H NMR (DMSO-d_6) spectrum of fused pyridine system **5** revealed the presence of two singlet signals at δ 13.15 and 12.60 ppm characteristic for 2NH (pyrimidine NH). Another doublet signal at δ 8.90 ppm was assigned for one pyridine proton (CH-N). Whereas, the ^{13}C NMR (DMSO-d_6) spectrum displayed a signal at δ 176.55 ppm corresponding to C=S and a signal at 160 ppm for the carbonyl group. Moreover, the mass spectrum of compound **5** showed a peak at *m/z*=305 (19%) corresponding to the molecular ion peak.

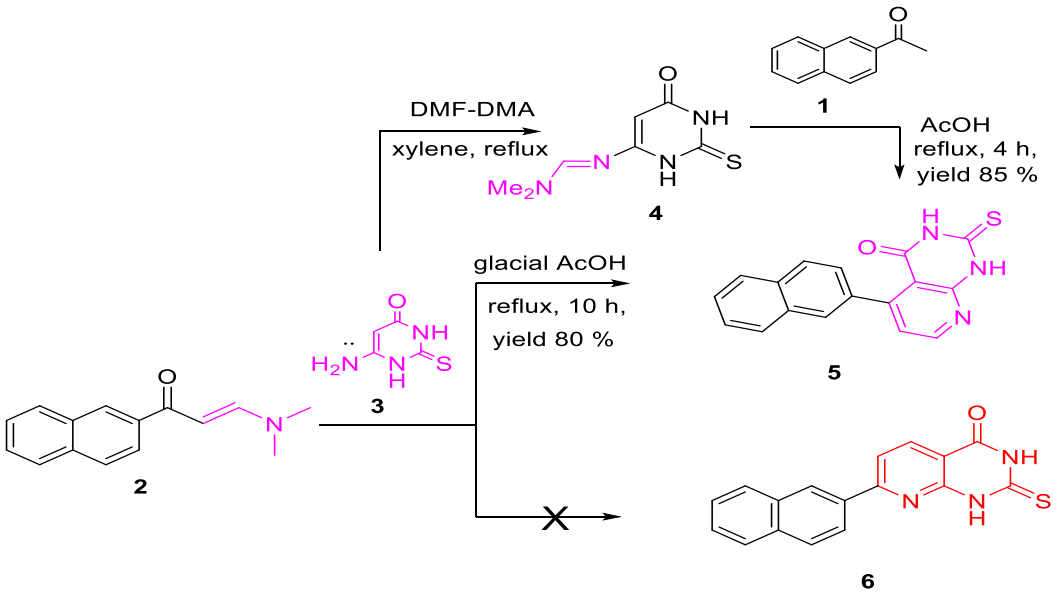

Scheme 2. Synthesis of 2-thioxopyrido[2,3-d]pyrimidine-4(1H)one derivative (5)

Scheme 3 gives an illustration for reaction of bi-nucleophile reagent with enaminone **2** to obtain thioxopyridopyrimidinone derivative **5**. The product **5** is obtained by the first nucleophilic addition of amino group to the enaminone double bond, followed by intramolecular oxidative cyclization and the loss of dimethylamine and water molecules, respectively (**Scheme 3**).

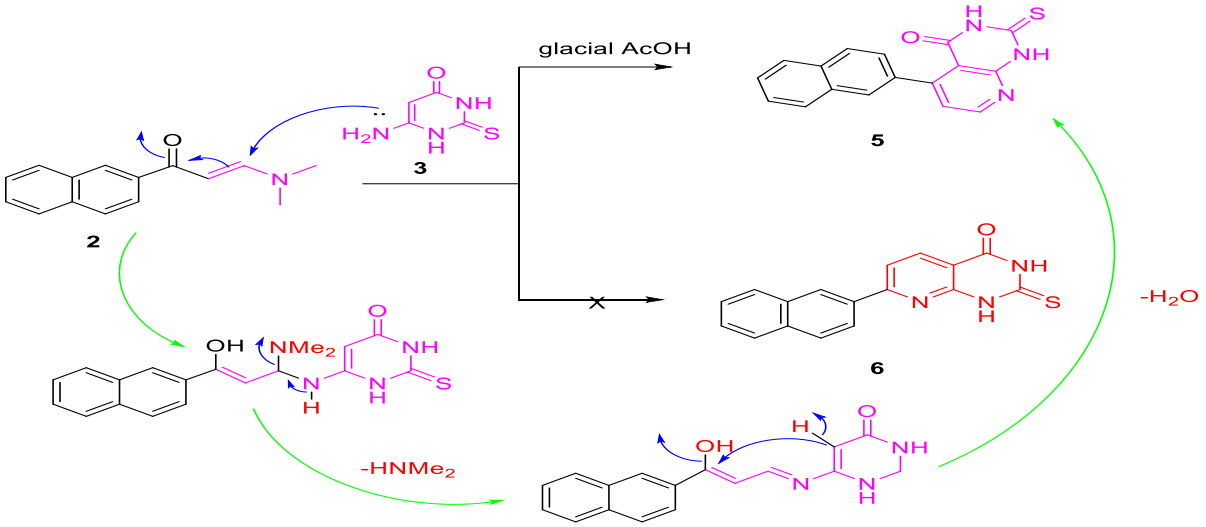

Scheme 3. Mechanism of Synthesis of 2-thioxopyrido[2,3-d]pyrimidine-4(1H)one derivative (5)

According to literature [23], hydrazonoyl halides belong to the most pertinent reagents for synthesis of different series of substituted pyrazoles. However, it was reported that substituted pyrazoles had potent biological activities against different diseases [24- 27]. Here, we've synthesized a series of substituted pyrazoles through the reaction of enaminone **2** in dry benzene with *C*-acetyl–*N*–arylhydrazonoyl chlorides (**7a–c**) and/or (*C*–ethoxycarbonyl)–*N*–arylhydrazonoyl chlorides (**7d, e**) in the presence of triethyl amine (**Scheme 4**). The yield of the reaction varied from moderate to good by changing the substitution on the benzene ring. Compound **8b** showed the highest yield 85%. The reaction reactivity of hydrazonoyl chloride derivatives **7a-e** toward the enaminone increases with the presence of electron-donating group on the benzene ring. It increase the nucleophilicity of the amine group. The chemical structure of tri-substituted pyrazoles **8a–e** was substantiated from its spectral data and elemental analysis. For instance, ^{1}H NMR spectrum of compound **8d** showed triplet signal at δ 0.97ppm for CH_3, quartet signal at δ 4.06 ppm for CH_2 protons and singlet signal for pyrazole-H proton at δ 9.15 ppm. Moreover, ^{13}C NMR (DMSO-d_6) spectrum displayed two signals at 161 and 188 ppm corresponding to two carbonyl groups. Scheme 4 shows the formation of pyrazole derivatives **8a-e** *via* 1,3-dipolar cycloaddition of nitrilimine intermediates, generated *in-situ* from hydrazonoyl chlorides in the presence of triethyl amine, to enaminone **2**. After replacing the chloride atom of the hydrazonoyl chloride **7a-e** with a nucleophilic group of the dipolarophile, an intramolecular cyclization occurs to afford the target compounds (**8a-e**).

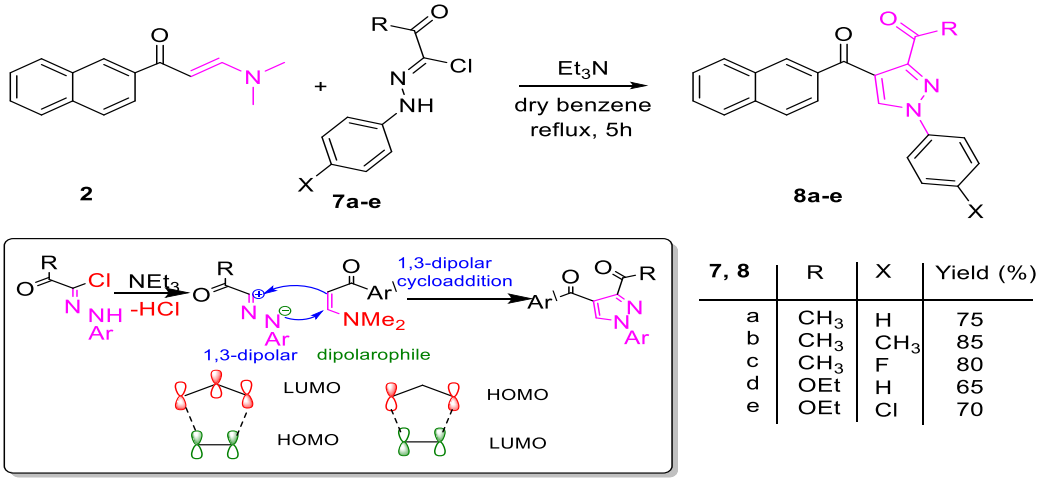

7, 8	R	X	Yield (%)
a	CH_3	H	75
b	CH_3	CH_3	85
c	CH_3	F	80
d	OEt	H	65
e	OEt	Cl	70

Scheme 4. Mechanism and reaction of enaminone 2 with hydrazonoyl chloride derivatives (7a-e)

It was noted that, pyrazole derivative **8a** was reported as as a precursor for preparation of many anticancer agents by Dawood and co-workers [28]. However, the potent biological activity of pyrazole bases encouraged us to study the antiviral activity for all synthesized pyrazole derivatives. The selectivity index SI ((CC_{50}) / (IC_{50})) of the tested compounds was obtained after assigning the cytotoxicity concentration CC_{50} and inhibitory concentration IC_{50}. Indeed, compound **8a** showed good antiviral activity. It demonstrated selectivity index (SI) equal to 12. It has auspicious antiviral activity results against SARS-COV 2. In addition, compounds **8b** and **8d** showed promising antiviral activity with highest selectivity. Compound **8b** exhibited selectivity index (SI) equal 21.98 while compound **8d** showed selectivity index (SI) equal to 27.73. According to Molecular electrostatic potential (MEP) calculations to predict the electrophilic and nucleophilic attack sites in the optimal configuration of the compounds tested (**8b**, **8d**, and Remdesivir), which is highly valuable in molecular structure research. The target derivatives **8b,d** exhibit a substantial number of positive and negative regions in their MEP, which play a significant role in their interactions with biological targets. In the frontier molecular orbital (FMO), Compounds with a small energy gap between their orbitals are unstable and highly reactive and this applies to compound **8b,d**. Chemically reactive compounds (**8b**, and **8d)** are more pliable and less rigid than remdesivir, indicating that they are also more reactive overall. In addition, the results of molecular docking in **Table 3** clearly show that when docking with SARS-CoV-2 spike glycoprotein (PDB ID: 6VSB) subunit B, the binding energy (ΔG) for the more powerful compounds **8b,d** was greater than that of the most commonly reported drugs such as Ribavirin, Mycophenolic acid, Chloroquine, and Isoniazid, but was near to that of Ritonavir and Hydroxychloroquine. The binding energy of **8b,d** was greater than that of Oseltamivir, Ribavirin, Mycophenolic acid, Chloroquine, Hydroxychloroquine, and Isoniazid medicines during the docking procedure against SARS-CoV-2 spike glycoprotein (PDB ID: 6VSB) subunit C. The results of this comparison suggest that the two compounds with the highest potency (**8b,d**) may have the ability to inhibit SARC-CoV-2.

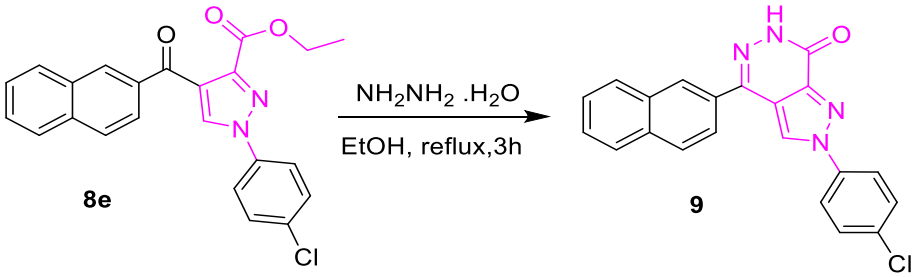

Scheme 5. hydrazinoylsis of (8e).

Refluxing of recently synthesized pyrazole derivative **8e** with hydrazine hydrate for 2 hours afforded pyrazolo[3,4-d]pyridazine derivative **9** (**Scheme 5**). The spectroscopic and micro analytical data supported the structure of compound **9**. The IR spectrum of compound **9** showed absorption bands (ν, cm^{-1}) at 3139 and 1674 cm^{-1} representing NH and C=O groups, respectively. However, the ^{1}H NMR (DMSO-d_6) spectrums of **9** displayed signals at δ (ppm): 9.63 (s, 1H, H-pyrazole), 12.38(s, 1H, NH). The mass spectrum revealed a molecular ion peak at m/z = 338 (45%).

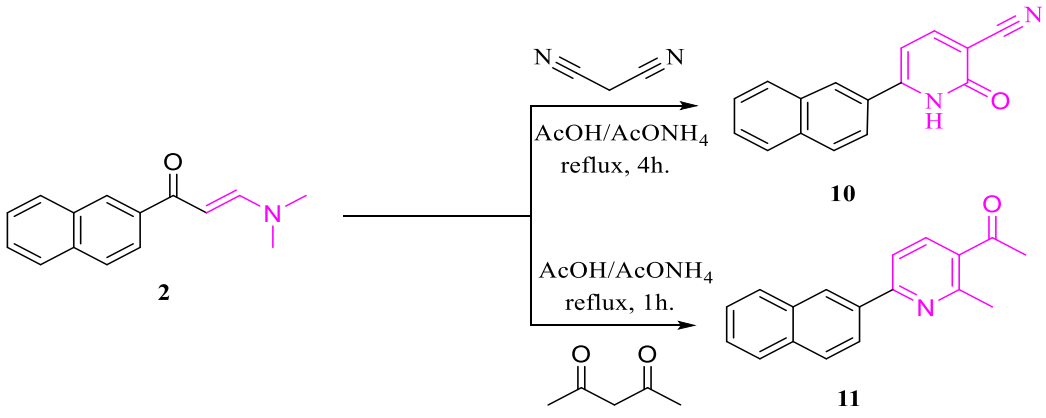

Scheme 6. Synthesis of 6-naphthyl-2,3-disubstituted pyridine (10) and (11)

It is well known that the carbanions of active methylene substances, such as nitriles, 1,3-diketones, and *β*-keto esters, are particularly useful for preparing biologically active components and are good starting points for building substituted pyridine moieties **(Scheme 6).** In 2009, Osama Ahmed et al [29] synthesized 6-(naphthalen-2-yl)-2-oxo-1,2-dihydropyridine-3-carbonitrile **10** by the reaction of sodium salt of 1-naphthyl-3-hydroxy-2-propene-1-one with cyanamide in 85% yield. In the current work, different method was used to prepare the same compound. Accordingly, treatment of enaminone **2** with active nitrile, specifically malononitrile in refluxing acetic acid and in the presence of ammonium acetate for 4 hours to afford the substituted pyridine derivative **10** in 75% yield (**Scheme 6)**. The IR spectrum of compound **10** exhibited absorption bands at (*v*, cm^{-1}): 3349 (NH), 2215 (CN), 1648 (C=O) groups. Moreover, ^{13}C NMR (DMSO-d_6) spectrum of **10** revealed signals at δ 117 and 165.19 ppm are characteristic for CN and C=O groups, respectively. The mass spectrum assigned a molecular ion peak at m/z= 246 (17%). The activity of enaminone **2** was confirmed by the reaction with 1, 3-diketones that is employed in the preparation of *N*-hetero-substituted pyridine systems and is recognized as a multifunctional building core. Thus, treatment of enaminone **2** with acetyl acetone afforded the desired biologically active substituted pyridine **11** in glacial acetic acid and in the presence of ammonium acetate for 1 hour to give a sole product in 85% yield identified by TLC **(Scheme 6).** It is important to note that, Elnagdi *et al* reported the preparation of compound **11** using the same condition [30]. The spectral analyses provided complete support for the structures of the pyridine derivatives **11**. For instance, the infrared spectrum of compound **11** revealed an absorption band at (*v*, cm^{-1}): 1679 corresponding to (C=O) group. ^1H NMR (DMSO-d6) showed singlet signals at δ 2.60 and 2.73 ppm for two methyl groups, respectively. Besides, the mass spectrum showed molecular ion peak at m/z= 261(58%). Moreover, the appearance of signal at δ 200.32 ppm was assigned to the carbonyl group in ^{13}C NMR spectra. Following that, 1,3-binucleophlic amino heterocyclic amines play a crucial role as building blocks for the synthesis of condensed pyrimidine heterocycles [27]. Owing to the broad spectrum in biological activity associated with condensed azolopyrimidines, a large number of interested studies were reported. Therefore, treatment of enaminone **2** with 3, 5-diamino-1*H*-1,2,4-triazole and 1*H*-benzo[*d*] imidazole-2-amine in refluxing glacial acetic acid for 10 hours to afford the corresponding fused azolopyrimidines **12** and **13**, respectively **(Scheme 7).**

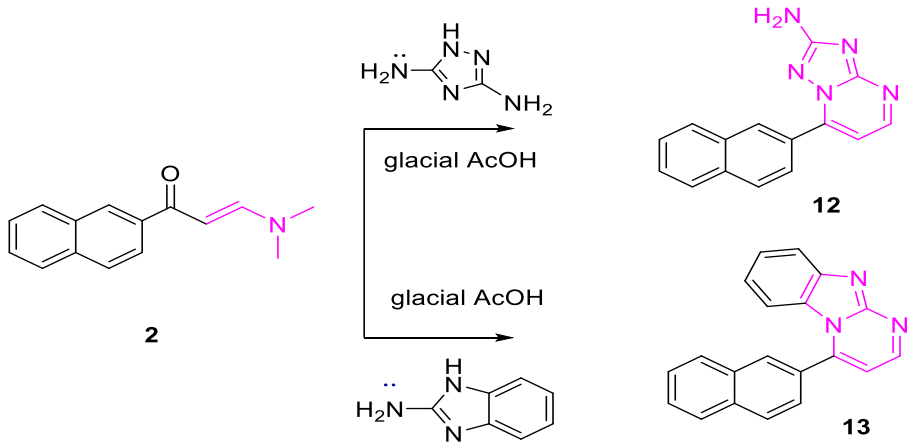

Scheme 7. Synthesis of [1,2,4] triazolo[1,5-a] pyrimidine (12) and [4,5]imidazolo[1,2-a] pyrimidine (13)

The newly synthesized triazolopyrimidine and imidazolopyrimidine derivatives **12, 13** were identified through their spectral data and elemental analysis. IR spectra of compounds **12** and **13** showed disappearance of the stretching peak of carbonyl group of enaminone **2**. However, ^1H-NMR (DMSO-d_6) spectrum of compound **12** showed broad signal at δ 4.3 ppm for NH_2-protons and singlet signal at δ 8.76 ppm in the aromatic region corresponding to H-naphthalene. The mass spectrum of compound **13** showed base peak, at m/z= 261 (100%) corresponding to molecular ion peak. Also, the ^1H-NMR (DMSO-d_6) of compound **13** showed two signals appeared as doublet at 8.17 and 8.95 ppm for two H-pyrimidine whereas, the mass spectrum showed a molecular ion peak at m/z=295(44%).

2.2 Biological Activity

2.2.1 Antiviral Activity

The antiviral activity of the synthesized pyridine and pyrazole derivatives against SARS-CoV-2 strain hCoV-19/Egypt/NRC-03/2020 was tested by the crystal violet assay (**Fig. 3** and **Table 1**). The results revealed that the tested compounds displayed activity within the range of low inhibition to moderate inhibition to high inhibition. While compounds **5**, **8c** and **8e** showed low inhibition activity at all safe dose concentrations. The compounds **9**, **11** and **12** articulated moderate inhibition activity, whereas compounds **8a**, **8b** and **8d** gave high inhibition activity.

Table 1. Antiviral activity of the new synthesized derivatives against SARS-CoV-2.

Sample code	CC_{50} µMol/ml	IC_{50} µMol/ml	SI (CC_{50} / IC_{50})
5	**573.8**	**230.7**	**2.49**
8a	**580.4**	**48.3**	**12**
8b	**572.9**	**26.06**	**21.98**
8c	**578.2**	**169.1**	**3.4**
8d	**570.1**	**20.56**	**27.73**
8e	**568.8**	**419.8**	**1.35**
9	**503.3**	**84.99**	**5.9**
11	**479.2**	**50.7**	**9.45**
12	**559.5**	**63.55**	**8.8**

2.2.1.1 Cytotoxicity concentration 50 (CC_{50}):

We have examined the cytotoxicity of these tested compounds on Vero-E6 cell lines to determine the safe doses that we can use later without any toxic side effects resulting from the toxicity of these compounds. We found that the cytotoxicity concentration 50 (CC_{50}) of these examined compounds ranges between 479.2 and 580.4 µMol/ml. This means that these compounds (analogs) are largely safe, allowing us to use them comfortably at concentrations close to those obtained. The Pyrazole, Pyridine and condensed pyrimidine derivatives have a limited range of cytotoxicity concentration 50% (CC_{50}) for VERO-E6 cells that ranged from 580.4µMol/ml to 479.2µMol/ml for **11** and **8a,** respectively.

2.2.1.2 Inhibitory concentration 50 (IC_{50}):

We determined the inhibitory concentration 50 (IC_{50}) of fifty percent of the virus using the compounds individually, to find in the end that the inhibitory concentration of the nine compounds ranged between 20.6 and 419.8 µMol/ml. This means that the efficiency of the nine compounds is not the same, and this matches the selectivity index, which clearly shows this. The Pyrazole, Pyridine and condensed pyrimidine derivatives have a broad range of inhibitory concentration 50% (IC_{50}) for SARS-CoV-2 virus that ranged from 20.56µMol/ml to 419.8µMol/ml for **8d** and **8e,** respectively.

2.2.1.3 Selectivity Index (SI):

After assigning both Cytotoxicity concentrations 50 (CC_{50}) and Inhibitory concentrations 50 (IC_{50}), we had obtained the selectivity index SI ((CC_{50}) / (IC_{50})). Therefore, according to the selectivity index, we divided the nine compounds into three categories:

●Class I: limited inhibition ●Class II: moderate inhibition ●Class III: promising inhibition In conclusion, we only had 3 promising analogues out of 9 compounds. Pyrazole, Pyridine and condensed pyrimidine derivatives contain a wide range of selectivity index SI ((CC_{50}) / (IC_{50})), which ranges from 27.73 to 1.35 for **8d** and **8e** respectively. This indicates that **8d** has promising activity as an anti-SARS-CoV-2 virus, while **8e** had very limited activity as anti-SARS-CoV-2 virus. The active compounds expressed themselves through the crystal violet assay and their selectivity index was higher than 10, it ranged between 12 and 27.7 Therefore, they were described as effective and promising. Compounds with a selectivity index values that are less than 10 is described to be moderate or limited inhibition.

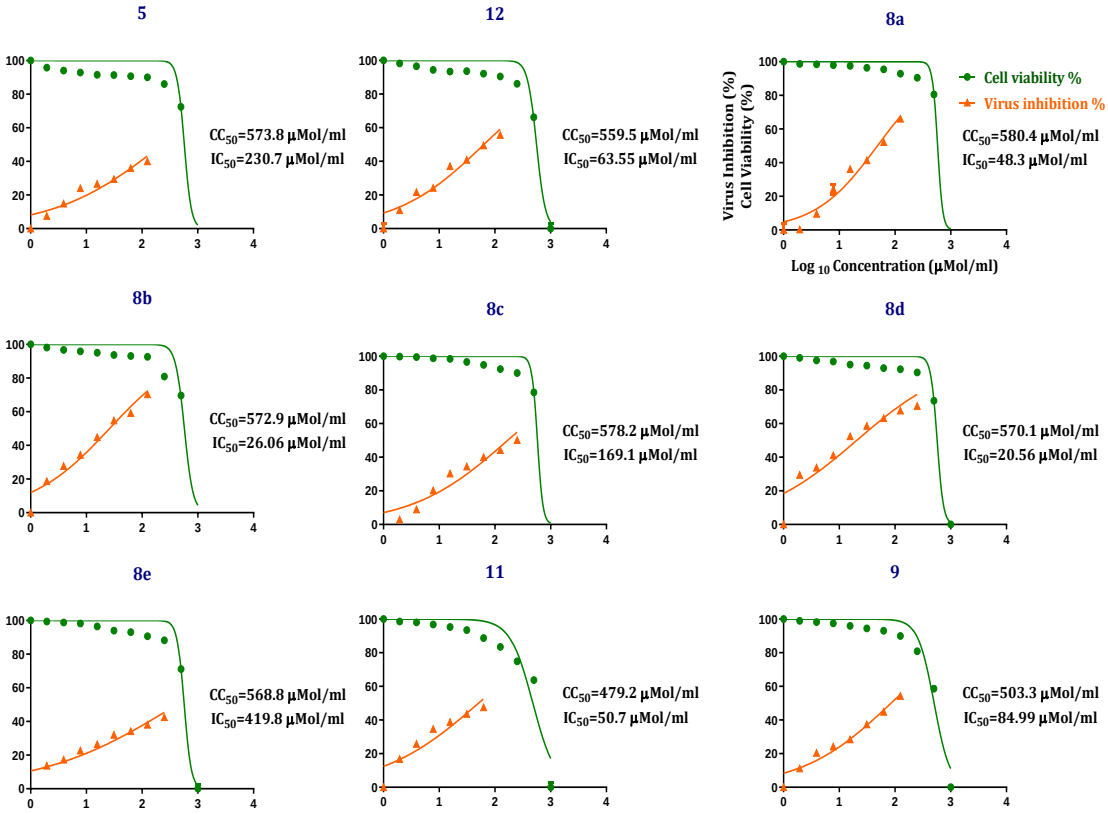

Fig. 2. CC_{50}, IC_{50} and SI for new Pyrazole, pyridine and condensed pyrimidine derivatives

2.3 Structure Activity Relationship (SAR) Study

To **correlate the relation between the chemical structure of the synthesized compounds with their anti-viral activities, structure activity relationship will be discussed as visualized in** fig 3**. In general, Most of the newly synthesized compounds exhibited moderate to strong antiviral activity against SARS-COV-2. Pyrazole derivatives** 8a**,** 8b **and** 8d **showed strong antiviral activity than that observed in pyridine and condensed pyrimidine heterocycles** 5**,** 9**,** 11**,** 12**. compound** 8d **(R =** OEt **and** X = Cl**) showed the most antiviral activity against SARS-CoV-2 virus with selectivity index (SI= CC_{50} / IC_{50}) equale to 27.73 while compound** 8b **(R =** CH_3 **and X =** CH_3**)exhibited selectivity index equal to 21.9. The third compound is** 8a **(R =** CH_3 **and X = H) with selectivity index equal to** 12 **as showen in table (1). Hence the presence of ester group of compounds** 8d **in postion 3 of pyrazole ring enhance the activity as antiviral agent than keton group (i.e.** 8a & 8b**), on the other hand the presence of halogen group in aryl group attached in postion 1 of pyrazole ring deactivate the antiviral property (i.e.compounds** 8c & 8e**) The noncondensed pyridine ring showed moderate activity than noncondensed pyrazole ring as the more nitrogenated ring showed high activity, (i.e. compound** 8 **higher activity than compound** 11**), finally, condesed ring pyrazole or triazol rings showed lower antiviral activity against SARS-COV-2, (i.e compound** 9 &12**)**

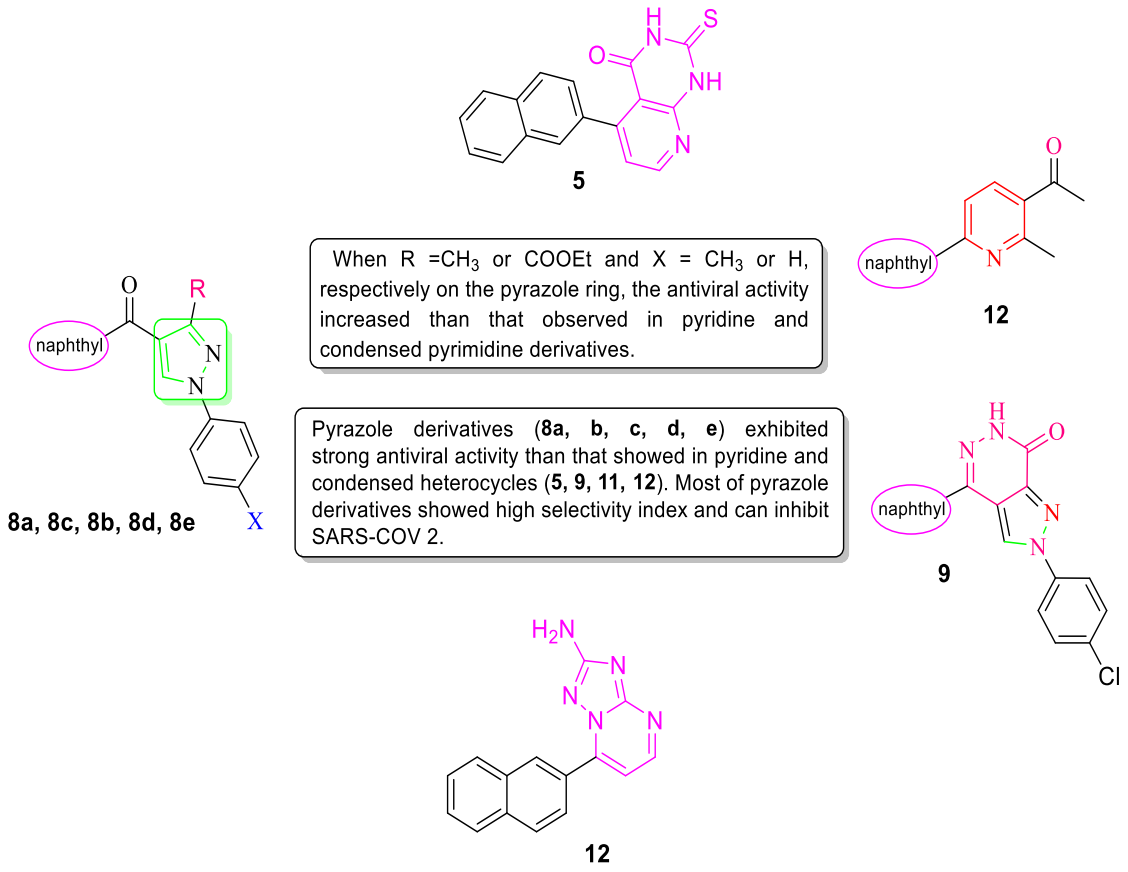

Fig. 3. Structure activity relationship study of synthesized pyrazole, pyridine and condensed diazole derivatives (5-12)

2.4. DFT parameters.

2.4.1. Molecular electrostatic potential (MEP).

Utilizing color grading, MEP was calculated to predict the electrophilic and nucleophilic attack sites in the optimal configuration of the compounds tested (**8b**, **8d**, and Remdesivir), which is highly valuable in molecular structure research. The B3LYP was used to generate the MEP map, with the optimal results obtained from the 6-31G(d,p) basis set. As we go from red to orange to yellow to green to blue, the potential grows. An excellent spot for electrophilic attack is shown by the red zone, which indicates the largest negative area. The blue area represents the most positively charged spot, which is ideal for nucleophilic attack. The color green represents a potential middle ground between the two extremes (red and dark blue). In between the two extremes, green for moderate and red/dark blue for extreme, you have the zone yellow and light blue.

From **figure (4),** The electron-rich areas are represented at the oxygen of carbonyl group of **8b**, **8d**, and remdesivir, also at the oxygen of -OCH_2CH_3 in **8d**. However, an electron deficiency region is located at the nitrogen of NH_2 for remdesivir, at CH_3, and CH- of benzene ring for **8b**, also at hydrogens of -OCH_2CH_3, and CH-of benzene ring for **8d**. Moreover, the yellow color appears on nitrogen's of pyrazole ring for **8b,d**, and at nitrogen of nitrile group for remdesivir. The green color appears on benzene, and naphthalene rings at **8b,d**, and at benzene ring in remdesivir, that characterized neutral sites. The target derivatives **8b,d** exhibit a substantial number of positive and negative regions in their MEP, which play a significant role in their interactions with biological targets. These findings corroborate a molecular docking investigation in which hydrogen bonds (donors or acceptors) formed between these regions and the active site located in the pocket of the target protein, as illustrated in the accompanying table (4).

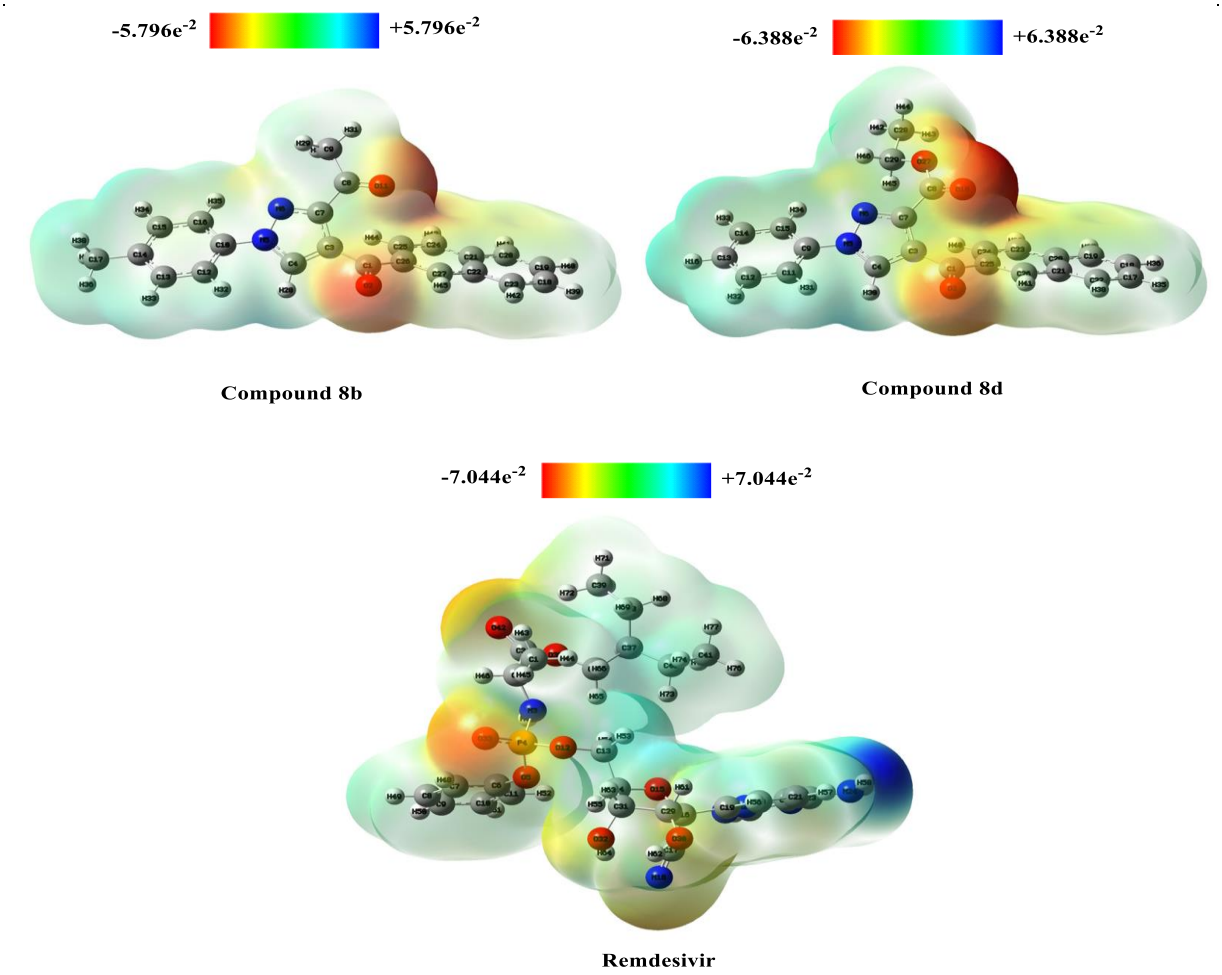

Fig. 4. MEP map of compounds 8b, 8d, and Remdesivir.

2.4.2. Frontier molecular orbitals

The frontier molecular orbitals (FMOs) are utilized to estimate chemical reactivity and kinetic stability using quantum chemistry calculations [31, 32]. LUMO represents the electron-accepting capability (empty state), whereas HOMO denotes the electron-donating capability of a molecule (complete stage). Assigning a single electron from HOMO to LUMO is responsible for coordinating the transition from the ground state to the first excited state [33]. An increase in kinetic stability is observed as the HOMO-LUMO gap expands. A visual depiction of FMOs is seen in **figure (5).** The energy values are E_{HOMO} = (-0.2144, -0.2159, & -0.2262) eV, E_{LUMO}= (-0.0629, -0.0635, & -0.0456) eV and energy gap is $\Delta \boldsymbol{E}$ = (0.1515, 0.1524, & 0.1806) eV for compounds **8b**, **8d**, and Remdesivir, respectively.

Using HOMO, and LUMO orbital energies, the electronegativity (χ), electrophilic index (ω), chemical hardness (η), and chemical softness (S) of compounds **8b**, **8d**, and remdesivir can be calculated as:

$$X = -1/2\ (E_{HOMO} + E_{LUMO}) \quad (1)$$

$$\eta = -1/2\ (E_{HOMO} - E_{LUMO}) \quad (2)$$

$$S = 1/\eta = -2\ (E_{HOMO} - E_{LUMO}) \quad (3)$$

$$\omega = X^2/2\eta \quad (4)$$

Table 2. DFT parameters calculated for the synthesized compounds 8b, 8d, and remdesivir.

Molecular Descriptors.	Dipole moment, μ (Debye)	E_{HOMO} (eV)	E_{LUMO} (eV)	$(H - L)$ ΔE gaps (eV)	X (eV)	η (eV)	S (eV^{-1})	ω (eV)
8b	5.0304	-0.2144	-0.0629	0.1515	0.1386	0.0757	13.2013	0.1268
8d	5.8101	-0.2159	-0.0635	0.1524	0.1397	0.0762	13.1233	0.1280
Remdesivir	7.4108	-0.2262	-0.0456	0.1806	0.1359	0.0903	11.0741	0.1022

HOMO, highest occupied molecular orbital; LUMO, lowest unoccupied molecular orbital. X = Electronegativity, η = Chemical hardness, S = Chemical softness, ω = Electrophilic index.

Using the data in **table (2),** the tendency of electrons to exit a stable system is described by the electronegativity values of χ = (0.1386, 0.1397, & 0.1359) eV for compounds **8b**, **8d**, and remdesivir, respectively. The chemical hardness values for **8b**, **8d**, and remdesivir are η = (0.0757, 0.0762, & 0.0903) eV, respectively. The hardness measures the resistance to altering the electron distribution and relates to the reactivity of the chemical system. The electrophilicity index values are ω = (0.1268, 0.1280, & 0.1022) eV, respectively, which were measured as the energy reduction caused by the maximum electron flow between the acceptor and the donor. The energy gap provides insight into the chemical stability and reactivity of the compounds, as estimated from the reactivity descriptors in the table. Compounds with a small energy gap between their orbitals are unstable and highly reactive. Chemically reactive compounds (**8b**, and **8d)** are more pliable and less rigid than remdesivir, indicating that they are also more reactive overall.

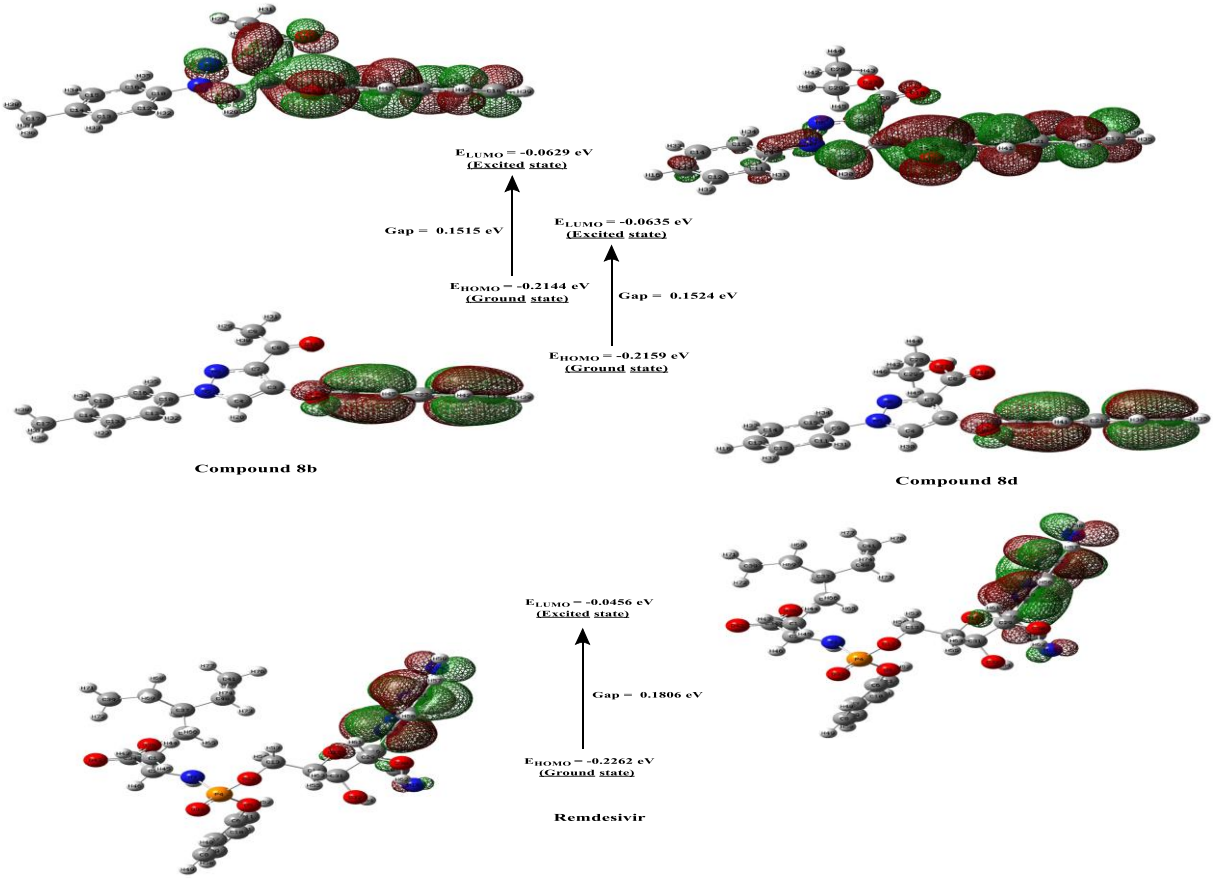

Fig. 5: The contour plots of HOMO and LUMO orbitals of compounds 8b, 8d, and remdesivir.

2.5. Visualization of docking results.

In this study we are utilizing the molecular docking method to study the efficiency of the target derivatives (**5, 8a-e, 9, 10, 11, 12 and 13**) as inhibitors of SARS-CoV-2 spike glycoprotein (PDB ID: 6VSB).The results obtained from these docking studies indicated strong interactions of compounds (**5, 8a-e, 9, 10, 11, 12 and 13**) with (6VSB) of SARS-CoV-2. The binding energy calculated varied in the range of (-3.4 to -5.8 kcal/mol) with (6VSB.B), and in the range of (-4.5 to -5.7 kcal/mol) with (6VSB.C), suggesting that the synthesized molecules can spontaneously interact within the binding site of the SARS-CoV-2 selected receptors.

2.5.1. Docking on the receptor SARS-CoV-2 spike glycoprotein (PDB ID: 6VSB) subunit B.

The results of docking the promising compounds (**5, 8a-e, 9, 10, 11, 12 and 13**) with SARS-CoV-2 spike glycoprotein (PDB ID: 6VSB) subunit B showed significant interactions and binding of the compounds with the target protein (**Table 3& 4**). The binding energies (ΔG) of the more potent compounds (**8a**, **8b**, **8d, 8e**) are −5.5 Kcal/mole, −5.6 Kcal/mole, −5.8 Kcal/mole, and −5.5 Kcal/mole; respectively.

All tested derivatives form hydrogen bonds and hydrophobic interactions with amino acids of subunit B. The amino acids formed the hydrogen bonds and hydrophobic reactions with the tested compounds were different. The several amino acids in subunit B which had vital role, are Ala 522, Gln 564, Leu 517, Gly 545, Pro 521, Asn 544, Leu 546, Leu 518, Arg 577, and Phe 392. Compound **8b** revealed one hydrogen bond with Ala 522 and two pi-H contacts with Leu 546 (**Fig. 6**). Compound **8d** stabilizes the connection with SARS-CoV-2 spike glycoprotein (PDB ID: 6VSB) subunit B within two H-bonds with Arg 577 and Ala 522 amino acids. In addition, the compound showed pi-H interaction with Leu 546 (**Fig. 7**).

2.5.2. Docking on the receptor SARS-CoV-2 spike glycoprotein (PDB ID: 6VSB) subunit C.

The docking experiments on the target protein demonstrated that the synthesized compounds have comparable orientations inside the active pocket (**Table 3& 4**). The binding energies (ΔG) of the more potent compounds (**8a**, **8b**, **8d, 8e**) are -5.4 Kcal/mole, -5.7 Kcal/mole, -5.6 Kcal/mole, and -5.3 Kcal/mole: respectively. Many of the amino acids in subunit C which are involved in hydrogen bonding and hydrophobic interaction, are His 49, Leu 48, Ser 50, Lys 964, Lys 304, and Gln 957. Compound **8b** predicted binding pattern identified one hydrogen bond with Gln 957 amino acid residue. Further, two pi-H contacts with His 49 and Ser 50 (**Fig. 8**). Compound **8d** was coupled with the receptor protein by forming two hydrogen bonds with Ser 50, pi-H contact and pi-cation interaction with Lys 964 (**Fig. 9**).

In order to determine the inhibitory potential of the compounds (**5, 8a-e, 9, 10, 11, 12 and 13**) against the spike glycoprotein (PDB ID: 6VSB) subunits B and C of SARS-CoV-2, the binding energy (ΔG) values of the compounds that were tested were compared with the binding energy (ΔG) values of known antiviral drugs [34], including Ritonavir, Lopinavir, Remdesivir, Oseltamivir, Ribavirin, Mycophenolic acid (MPA), Chloroquine, Hydroxychloroquine (HCQ), Pemirolast, Isoniazid, and Eriodictyol (**table 3**).

As a result, **Table 3** clearly shows that when docking with SARS-CoV-2 spike glycoprotein (PDB ID: 6VSB) subunit B, the binding energy (ΔG) for the more powerful compounds **8b,d** was greater than that of the most commonly reported drugs such as Ribavirin, Mycophenolic acid, Chloroquine, and Isoniazid, but was near to that of Ritonavir and Hydroxychloroquine. The binding energy of **8b,d** was greater than that of Oseltamivir, Ribavirin, Mycophenolic acid, Chloroquine, Hydroxychloroquine, and Isoniazid medicines during the docking procedure against SARS-CoV-2 spike glycoprotein (PDB ID: 6VSB) subunit C. The results of this comparison suggest that the two compounds with the highest potency (**8b,d**) may have the ability to inhibit SARC-CoV-2.

Table 3: **Molecular docking data represented in terms of binding energy (ΔG) in Kcal/ mole for 6VSB.B & 6VSB.C with compounds 5, 8a-e, 9, 10, 11, 12 and 13 and drug ligands.**

Sr. No.	Compounds (drugs)	Binding energy ΔG(Kcal/Mol)	
		6VSB.B	6VSB.C
1	Ritonavir	-5.6	-7.0
2	Lopinavir	-6.2	-6.6
3	Remdesivir	-6.8	-6.2
4	Oseltamivir	-6.0	-5.4
5	Ribavirin	-5.5	-5.4
6	Mycophenolic acid	-4.8	-5.4
7	Chloroquine	-5.4	-4.8
8	Hydroxychloroquine	-5.6	-5.5
9	Pemirolast	-6.2	-6.3
10	Eriodictyol	-6.7	-7.6
11	Isoniazid	-4.4	-5.0
12	5	-5.4	-5.0
13	8a	-5.5	-5.4

14	8b	-5.6	-5.7
15	8c	-3.4	-5.2
16	8d	-5.8	-5.6
17	8e	-5.5	-5.3
18	9	-4.9	-5.2
19	10	-4.8	-4.7
20	11	-5.2	-4.6
21	12	-5.4	-4.5
22	13	-3.9	-5.0

Table 4. Docking results of compounds 5, 8a-e, 9, 10, 11, 12 and 13 against SARS-CoV-2 spike glycoprotein (PDB ID: 6VSB) subunits B and C active spots.

Comp.	Ligand	Receptor	Interaction	Distance (in A° from main residue)	E (Kcal/mol)
SARS-CoV-2 spike glycoprotein (6VSB.B) subunit B active spot					
5	6-ring 6-ring	Asn 544 Leu 546	pi-H pi-H	3.99 3.61	-1.1 -0.8
8a	O 15	Leu 518	H-acceptor	3.07	-0.7
8b	N 7 6-ring 6-ring	Ala 522 Leu 546 Leu 546	H-acceptor pi-H pi-H	2.58 4.54 4.00	1.2 -0.6 -0.9
8c	N 7	Ala 522	H-acceptor	2.77	-3.5
8d	C 19 N 7 6-ring	Arg 577 Ala 522 Leu 546	H-donor H-acceptor pi-H	3.11 3.00 3.76	-0.8 -3.8 -0.6
8e	O 11 6-ring	Leu 518 Leu 518	H-acceptor pi-H	3.03 3.58	-0.8 -0.6
9	O 23 O 23	Phe 392 Leu 518	H-acceptor H-acceptor	3.20 2.75	-0.7 -1.4
10	N 13 N 13 6-ring 6-ring	Ala 522 Gln 564 Leu 517 Leu 517	H-acceptor H-acceptor pi-H pi-H	2.93 3.34 4.33 4.06	-4.0 -0.8 -0.6 -0.8
11	O 28 6-ring	Ala 522 Leu 517	H-acceptor pi-H	3.06 3.84	-1.6 -1.3
12	5-ring	Leu 517	pi-H	4.11	-0.9
13	N 10	Pro 521	H-acceptor	3.18	-0.8
SARS-CoV-2 spike glycoprotein (6VSB.C) subunit C active spot					
5	N 1 S 16 S 16 6-ring 6-ring 6-ring 6-ring	His 49 Ser 50 Ser 50 His 49 Lys 964 Lys 964 Lys 964	H-donor H-acceptor H-acceptor pi-H pi-H pi-cation pi-cation	3.19 3.50 3.35 4.50 4.13 4.12 4.30	-1.2 -1.7 -2.4 -0.8 -0.7 -8.1 -1.1
8a	O 2 O 2 5-ring 6-ring 5-ring	Ser 50 Ser 50 His 49 Lys 964 Lys 964	H-acceptor H-acceptor pi-H pi-H pi-cation	3.12 2.88 4.28 4.26 4.15	-2.2 -1.7 -0.6 -0.6 -0.9

8b	C 4 6-ring 6-ring	Gln 957 His 49 Ser 50	H-donor pi-H pi-H	3.34 4.71 4.50	-1.0 -0.6 -1.0
8c	O 2 N 7 5-ring 5-ring	Leu 48 Lys 964 Lys 964 Lys 964	H-acceptor H-acceptor pi-H pi-cation	3.21 3.20 4.05 4.12	-0.9 -2.1 -0.9 -1.1
8d	O 2 O 2 6-ring 5-ring	Ser 50 Ser 50 Lys 964 Lys 964	H-acceptor H-acceptor pi-H pi-cation	3.10 2.88 4.26 4.10	-2.2 -1.9 -0.6 -1.7
8e	O 11 5-ring 5-ring	Ser 50 His 49 Lys 964	H-acceptor pi-H pi-cation	2.99 4.22 3.68	-0.9 -0.8 -4.0
9	6-ring 6-ring 6-ring 6-ring 6-ring	Lys 304 Lys 304 Lys 304 Lys 964 Lys 964	pi-H pi-H pi-H pi-H pi-H	4.34 4.53 4.53 3.98 4.27	-0.6 -1.1 -0.9 -0.8 -0.6
10	N 10 6-ring	His 49 Leu 48	H-donor pi-H	3.18 3.90	-1.6 -1.0
11	O 28 6-ring 6-ring	Lys 964 Lys 304 Lys 964	H-acceptor pi-H pi-H	3.09 4.39 3.72	-0.7 -1.2 -0.8
12	6-ring 6-ring 5-ring 6-ring	Ser 50 Lys 304 Lys 964 Lys 964	pi-H pi-H pi-H pi-cation	4.50 3.75 4.03 3.70	-1.7 -0.7 -0.8 -0.6
13	6-ring	Ser 50	pi-H	4.86	-0.8

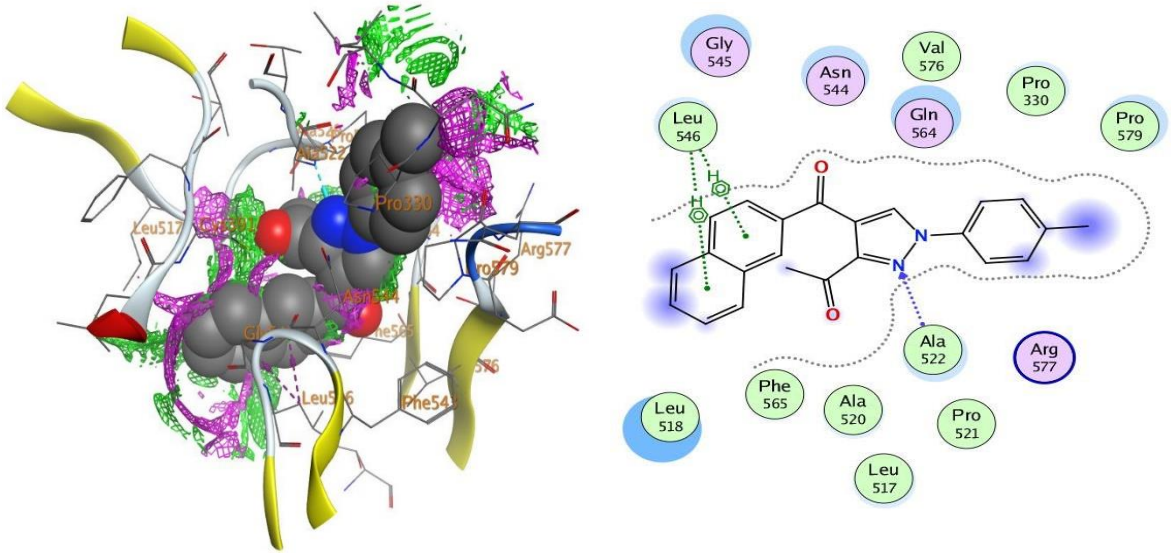

Fig. (6). 2D and the contact preferences of docked compound 8b into the active site of SARS-CoV-2 spike glycoprotein (PDB ID: 6VSB.B).

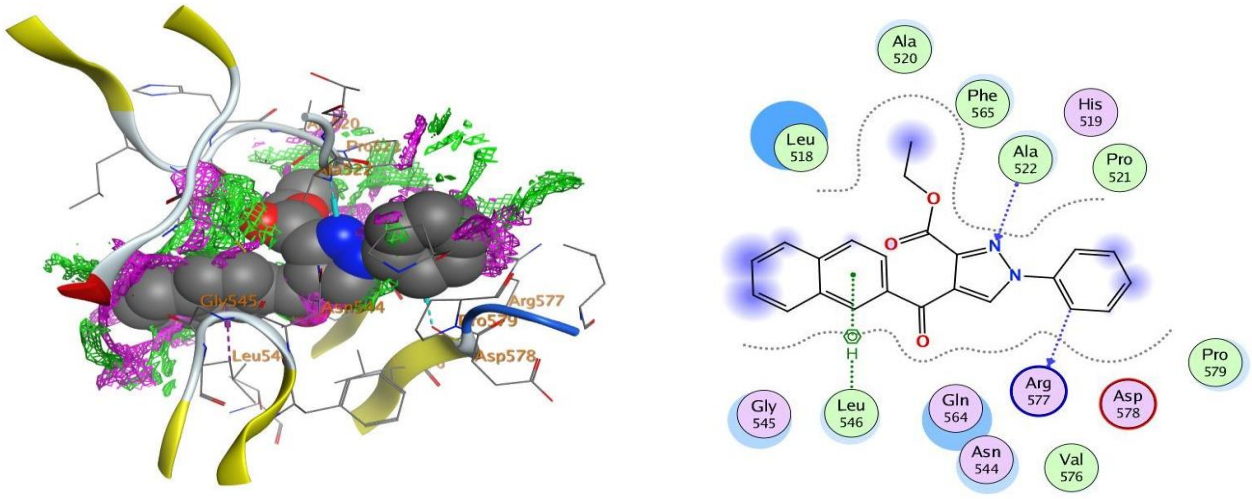

Fig. (7). 2D and the contact preferences of docked compound 8d into the active site of SARS-CoV-2 spike glycoprotein (PDB ID: 6VSB.B).

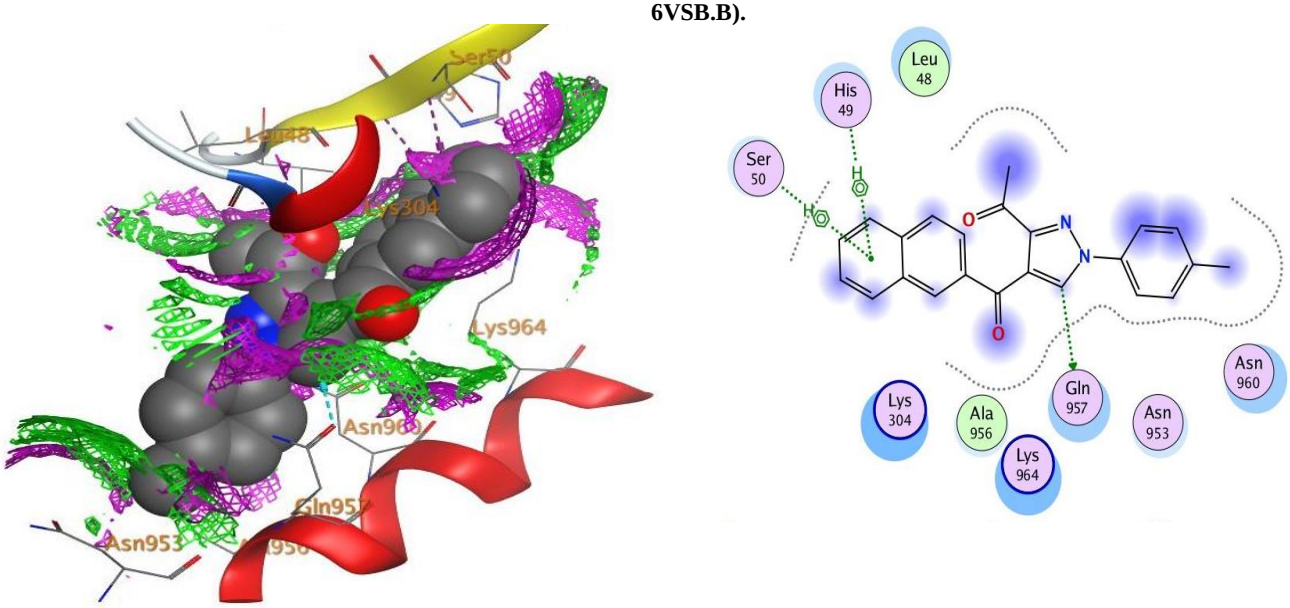

Fig. (8). 2D and the contact preferences of docked compound 8b into the active site of SARS-CoV-2 spike glycoprotein (PDB ID: 6VSB.C).

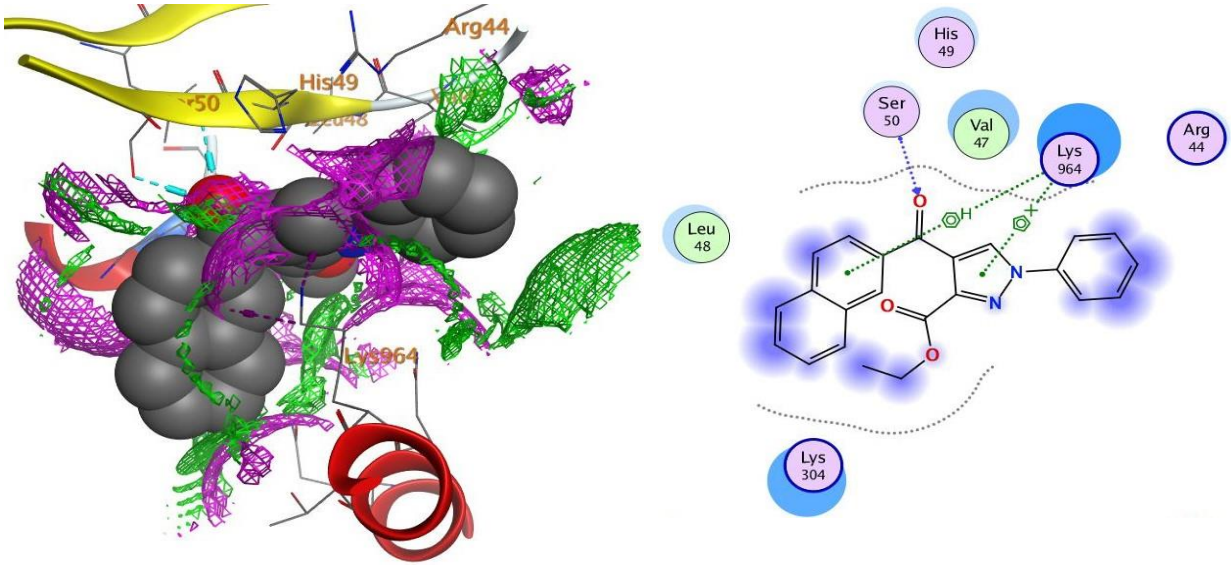

Fig. (9). 2D and the contact preferences of docked compound 8d into the active site of SARS-CoV-2 spike glycoprotein (PDB ID: 6VSB.C).

2.6. Pharmacophore studies.

With this strategy, we want to build and test a pharmacophore model (hypothesis) for COVID-19 drugs that utilize SARS-CoV-2 inhibitors [34]. To start, the eleven SARS-CoV-2 inhibitors (**table 5**) that will be utilized as training set compounds need to have their 3D structures built. Next, we give the pharmacophoric characteristics. The last step is to utilize the databases for the tested compounds (**8a**, **8b**, **8d**, and **8e**) that have the specified pharmacophoric qualities [35]. A compound's activity is related to the degree to which it maps to a built hypothetical model, which is expressed as the relative mobility of the query features relative to their matching ligand-target sites. Typical pharmacophoric features include hydrogen bond acceptors (Acc), donors (Don), charged or ionizable groups (Cat and Ani), hydrophobic (Hyd), metal ligators (ML), and aromatic rings (Aro). According to **table 6** and the figure (**fig. 10**), there are three parts to the preliminary pharmacophoric assessment

Table 5. PubChem standard drugs with chemical characteristics.

Pharmacophoric features	Structure features	Compound	Rmsd
F1: Hyd/Aro	Phenyl ring, CH_3.	**8a**	0.2115
F2: Acc/ ML	C=O, nitrogen of pyrazole ring.	**8b**	0.2065
F3: ML/Acc/ Don	C=O, nitrogen of pyrazole ring.	**8d**	0.2784
		8e	0.2760

Table 6. Pharmacophoric and structure features of the training inhibitors & rmsd values of the hitset.

Drugs	Molecular Formula	Molecular Weight	PubChem ID	CAS ID	Smile
Ritonavir	$C_{37}H_{48}N_6O_5S_2$	720.9	392622	155213-67-5	CC(C)C1=NC(=CS1)CN(C)C(=O)NC(C(C)C)C(=O)NC(CC2=CC=CC=C2)CC(C(CC3=CC=CC=C3)NC(=O)OCC4=CN=CS4)O
Lopinavir	$C_{37}H_{48}N_4O_5$	628.8	92727	192725-17-0	CC1=C(C(=CC=C1)C)OCC(=O)NC(CC2=CC=CC=C2)C(CC(CC3=CC=CC=C3)NC(=O)C(C(C)C)N4CCCNC4=O)O
Remdesivir	$C_{27}H_{35}N_6O_8P$	602.6	121304016	1809249-37-3	CCC(CC)COC(=O)C(C)NP(=O)(OCC1C(C(C(O1)(C#N)C2=CC=C3N2N=CN=C3N)O)O)OC4=CC=CC=C4
Oseltamivir	$C_{16}H_{28}N_2O_4$	312.40	65028	196618-13-0	CCC(CC)OC1C=C(CC(C1NC(=O)C)N)C(=O)OCC
Ribavirin	$C_8H_{12}N_4O_5$	244.20	37542	36791-04-5	C1=NC(=NN1C2C(C(C(O2)CO)O)O)C(=O)N
Mycophenolic acid	$C_{17}H_{20}O_6$	320.3	446541	24280-93-1	CC1=C2COC(=O)C2=C(C(=C1OC)CC=C(C)CCC(=O)O)O
Chloroquine	$C_{18}H_{26}ClN_3$	319.9	2719	54-05-7	CCN(CC)CCCC(C)NC1=C2C=CC(=CC2=NC=C1)Cl
Hydroxy Chloroquine	$C_{18}H_{26}ClN_3O$	335.9	3652	118-42-3	CCN(CCCC(C)NC1=C2C=CC(=CC2=NC=C1)Cl)CCO
Pemirolast	$C_{10}H_8N_6O$	228.21	57697	69372-19-6	CC1=CC=CN2C1=NC=C(C2=O)C3=NNN=N3
Eriodictyol	$C_{15}H_{12}O_6$	288.25	440735	552-58-9	C1C(OC2=CC(=CC(=C2C1=O)O)O)C3=CC(=C(C=C3)O)O
Isoniazid	$C_6H_7N_3O$	137.14	3767	54-85-3	C1=CN=CC=C1C(=O)NN

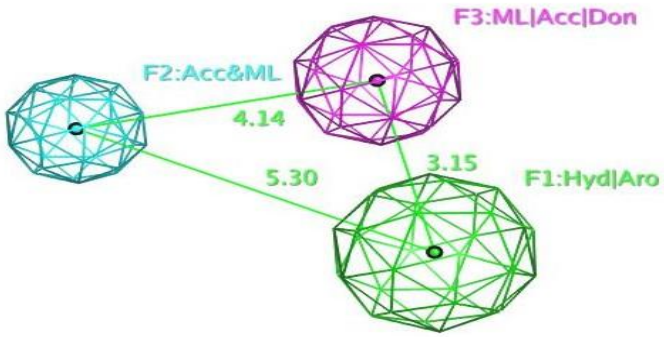

Fig. (10). Pharmacophore features and distances.

As can be shown in **table 6**, the rmsd's inhibitory influence grows stronger as it decreases. Superpositions of compounds **8a,b** exhibited the highest activity, with rmsd values of 0.2115 (**Fig. 11**) and 0.2065, respectively (**Fig. 12**)[24]. Compound **8d,e** exhibited strong inhibitory effects (rmsd values of 0.2784 and 0.2760, respectively) (**Fig. 13& 14**). This provides encouraging evidence of the antiviral activity's efficacy.

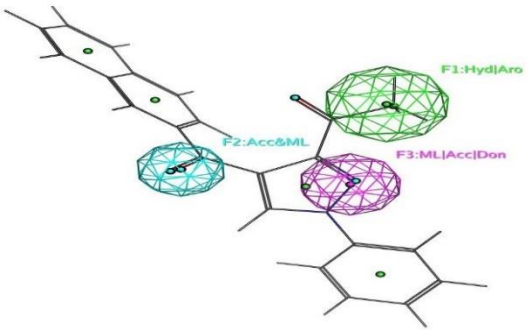

Fig. (11). Superposition of 8a with the query.

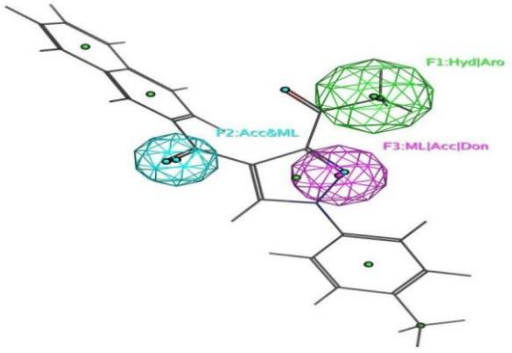

Fig. (12). Superposition of 8b with the query[22].

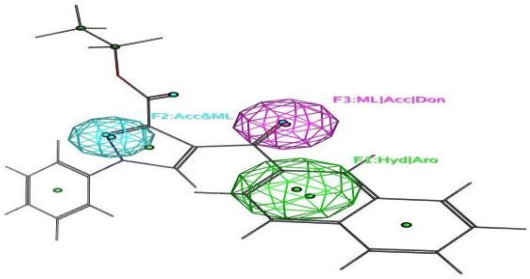

Fig. (13): Superposition of 8d with the query

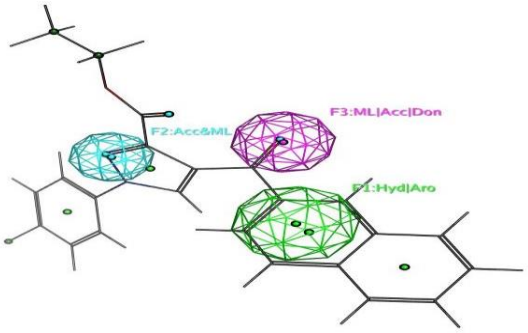

Fig. (14): Superposition of 8e with the query

3. Experimental

3.1. Chemistry.

Gallenkamp apparatus was used in measuring the melting points in open glass capillaries. Elemental analyses of the new structures were conducted at Cairo University Microanalytical Center. Potassium bromide disks were used for measuring the infrared spectra (IR), on a Pye-Unicam SP 3–300 and Shimaduz FTIR 8101 PC infrared spectrophotometer. Nuclear magnetic resonance spectra were carried out with a Varian Mercury (VXR-300 NMR spectrometer) at 75 MHz (^{13}C NMR) and at 300 MHz (^{1}H NMR). Mass spectra (EI) were measured at 70 eV using GC-MQP 1000 EX spectrometer from Shimadzu. Analytical TLC was carried out using Fluka precoated silica-gel 60,778 plates, and UV light (254 nm) was used to visualize the spots of new compounds.

***3-(Dimethylamino)-1-(naphth-2-yl)prop-2-en-1-one* (2)**

The preparation was achieved using the previously published procedure [6, 22, 28].

A mixture of 10 mmol of 3-acetyl naphthalene (1) and 15 mmol of N,N-dimethylformamide dimethylacetal (DMF-DMA) in 15 mL of dry xylene underwent reflux for 35h. The reaction mixture was left to cool and the precipitate that had developed was

filtered out and allowed to recrystallize in EtOH to obtain the pure product **2** as yellow crystals in yield (80 %). mp: 112-115 °C. ^{1}H-NMR (300 MHz, DMSO-d_6) δ (ppm): 2.96 (s, 3H, NCH_3), 3.15 (s, 3H, NCH_3), 5.98 (d, 1H, CH=, *J*=12 Hz), 7.54 (m, 2H, naphthalene-H), 7.75 (d, 1H, CH=, *J*=12.3 Hz), 7.92-8.04 (m, 4H, naphthalene-H), 8.50 (s, 1H, naphthalene-H).

Preparation of compounds 5.

To a solution of enaminone **2** (10 mmol) in glacial acetic acid (10 mL), 6-amino-thiouracil, was added. The reaction mixtures was refluxed for a 10 hours, and followed up by TLC. The mixtures was concentrated and allowed to cool at room temperature. The solid precipitates was filtered to obtain product **5**. The solid product was recrystallized from MeOH.

Second procedure for preparation of compound 5

In a round flask, *N*,*N*-dimethyl-*N*'-(6-oxo-2-thioxo-1,2,3,6-tetrahydropyrimidin-4-yl)formimidamide [22] (10 mmol) (**4**) in glacial acetic acid (10 mL), 2-aceyl naphthalene **1** (10 mmol) was mixed and the reaction mixture was refluxed for 4 hours. The mixture was cooled, and the precipitate filtered off, dried then recrystalized from MeOH to give **5** in 85% yield.

***5-(naphthalen-2-yl)-2-thioxo-2,3-dihydropyrido[2,3-d]pyrimidin-4(1H)-one* (5)**

Yield (80%), mp 138-139 °C (EtOH). IR (KBr, *v*, cm^{-1}): 3328, 3151(2NH), 1687 (C=O). ^{1}H-NMR (300 MHz, DMSO-d_6) δ (ppm): 7.53-7.65 (m, 3H, 3CH-naphthalene), 7.90-8.36 (m, 4H, 3CH-naphthalene+CH- pyrimidine), 8.68 (s, 1H, CH-naphthalene), 8.91 (d, 1H, CH-pyrimidine, *J*= 8.7 Hz), 12.60, 13.15 (2s, 2H, 2NH).^{13}C NMR (300 MHz, DMSO-d_6) δ (ppm):110.60 (C$^{\bullet}$-C=O), 117.01 (CH-pyridine), 124.08, 126.9, 127.59, 127.94, 128.73, 128.89 (CH-naphthalene), 134.43, 135.05, 137.16 (=C-naphthalene), 151.52 (-CH-N-pyridine), 159.44 (-C-C$^{\bullet}$-C-pyridine), 159.43 (-N-C-NH-), 163.84 (C=O), 176.05 (C=S). MS *m/z* (%): 305 [M^+] (19). 247 [M^+-NC=S] (18). Anal. Calcd for $C_{17}H_{11}N_3OS$ (305.36): C, 66.87; H, 3.63; N, 13.76. Found: C, 66.92; H, 3.65; N, 13.74.

General procedure for preparation of pyrazoles 8a-e

To a mixture of compound **2** (10 mmol) and the appropriate hydrazonoyl halides (**7**a-e) (1 mmol) in dry benzene (10 mL), a catalytic amount of TEA was added. The reaction mixtures were refluxed for 5 hours and reaction compilation was achieved by TLC. After reaction compilation, the solvent was removed by evaporation under reduced pressure to obtain pyrazole derivatives **8a–e** as white pure solid.

1-(4-(2-naphthoyl)-1-phenyl-1H-pyrazol-3-yl)ethan-1-one 8a .

Yield (75%), mp: 192-193 °C (EtOH). IR (KBr, *v*, cm^{-1}): 1685, 1648 (2C=O). ^{1}H-NMR (300 MHz, DMSO-d_6) δ (ppm): 2.59 (s, 3H, CH_3CO), 7.36-7.49 (m, 2H, Ar-H), 7.57-7.70 (m, 3H, CH-naphthalene), 7.94-8.10 (m, 6H, 3Ar-H+3CH-naphthalene), 8.41 (s, 1H, CH-naphthalene), 9.08 (s, 1H, H- pyrazole). ^{13}C NMR (300 MHz, DMSO-d_6) δ (ppm): 27.19 (CH_3), 119.44 (C$^{\bullet}$C=O pyrazole), 121.75, 122.88, 124.14, 127.12, 127.85, 128.57, 128.85, 129.83, 130.01, 130.57, 131.02, 131.15, 132.97, 134.57, 135.35, 136.65, 137.60 (CH-Ar), 150.14 (NC$^{\bullet}$$COCH_3$), 189.75, 193.07 (2C=O). MS *m/z* (%): 340 [M^+] (100). Anal. Calcd. for $C_{22}H_{16}N_2O_2$ (340.38): C, 77.63; H, 4.74; N, 8.23; Found: C, 77.68; H, 4.71; N, 8.22.

1-(4-(2-naphthoyl)-1-(p-tolyl)-1H-pyrazol-3-yl)ethan-1-one 8b

Yield (80%), mp: 218-220 ° C (EtOH). IR (KBr, *v*, cm^{-1}): 1685, 1648 (2C=O). ^{1}H-NMR (300 MHz, DMSO-d_6) δ (ppm): 2.37 (s, 3H, CH_3), 2.57 (s, 3H, CH_3CO), 7.38 (d, 2H, 2CH-Ar, *J*= 6 Hz), 7.58-7.67 (m, 2H, 2CH-Ar), 7.89-8.12 (m, 6H, 6CH-naphthalene), 8.40 (s, 1H, CH-naphthalene), 9.05 (s, 1H, H-pyrazole). ^{13}C NMR (300 MHz, DMSO-d_6) δ (ppm): 20.76 (CH_3-Ar), 27.35 (CH_3CO), 119.57, 122.98, 124.33, 127.12, 127.85, 128.57, 129.03, 130.01, 130.37, 131.62, 131.95, 132.32, 134.97, 135.35, 136.65 and 137.80 (C-Ar), 150.09 ($CH_3COC^{\bullet}$-pyrazole), 189.75 ($COCH_3$), 193.07 (CO). MS *m/z* (%): 354 [M^+] (100). Anal. Calcd. for $C_{23}H_{18}N_2O_2$ (354.41): C, 77.95; H, 5.12; N, 7.90. Found: C, 77.97; H, 5.11; N, 7.89.

1-(4-(2-naphthoyl)-1-(4-fluorophenyl)-1H-pyrazol-3-yl)ethan-1-one 8c

Yield (80%), mp 230-232 ° C (EtOH). IR (KBr, *v*, cm^{-1}): 1689, 1641 (2C=O). ^{1}H-NMR (300 MHz, DMSO-d_6) δ (ppm): 2.58 (s, 3H, CH_3CO), 7.46 (m, 2H, 2CH-Ar), 7.56 (m, 2H, 2CH-Ar), 7.94-8.12 (m, 6H, 6CH-naphthalene), 8.42 (s, 1H, CH-naphthalene), 9.07 (s, 1H, H-pyrazole). ^{13}C NMR (300 MHz, DMSO-d_6) δ: 27.12 (CH_3CO), 116.49 (C-pyrazole), 116.78, 121.75, 121.87, 122.88, 124.14, 126.84, 127.67, 128.39, 128.89, 129.93, 131.85, 132.14, 134.77, 135.19, 135.29 and 150.14 (C-Ar), 159.68 (C-pyrazole), 162.93 (FC-benzene), 189.33 ($COCH_3$), 192.27 (CO). MS *m/z* (%): 358 [M^+] (7), 357 [M^+-1] (28), 342 [M^+-CH_3] (38). Anal. Calcd. for $C_{22}H_{15}FN_2O_2$ (358.37): C, 73.73; H, 4.22; N, 7.82. Found: C, 73.79; H, 4.16; N, 7.80.

ethyl 4-(2-naphthoyl)-1-phenyl-1H-pyrazole-3-carboxylate 8d

Yield (65%), mp: 158-160 ° C (EtOH). IR (KBr, *v*, cm^{-1}): 1714, 1629 (C=O). ^{1}H-NMR (300 MHz, DMSO-d_6) δ (ppm): 0.97 (t, 3H, CH_3, *J*= 9 Hz), 4.06 (q, 2H, CH_2, *J*= 6 Hz), 7.36-7.63 (m, 5H, 3Ar-H+2H-naphthalene), 7.95-8.13 (m, 6H, 2H-Ar+4H-naphthalene), 8.48 (s, 1H, H-naphthalene), 9.15 (s, 1H, H-pyrazole). ^{13}C NMR (300 MHz, DMSO-d_6) δ (ppm):

13.69 (CH_3), 61.58 (CH_2), 121.34, 123.96, 124.23, 127.11, 127.81, 128.41. 128.87, 129.77, 129.88, 131.89, 132.08, 132.22, 132.35, 134.96, 135.23 and 137.55 (CH-Ar), 144.67 (C-pyrazole), 161.08 (COOEt), 188.46 (CO). MS *m/z* (%): 370 [M^+] (52), 326 [M^+-CH_3CH_2OH] (38). Anal. Calcd. for $C_{23}H_{18}N_2O_3$ (370.41): C, 74.58; H, 4.90; N, 7.56. Found: C, 74.65; H, 4.88; N, 7.51.

ethyl 4-(2-naphthoyl)-1-(4-chlorophenyl)-1H-pyrazole-3-carboxylate 8e

Yield (70%), mp 180-182 °C (EtOH). IR (KBr, *v*, cm^{-1}): 1714, 1629 (2C=O). ^{1}H-NMR (300 MHz, DMSO-d_6) δ (ppm): 0.95 (t, 3H, CH_3, *J*= 9 Hz), 4.04 (q, 2H, CH_2, *J*= 6 Hz) 7.35 (s, 1H, Ar-H), 7.61-7.68 (m, 4H, Ar-H+H-naphthalene), 7.95-8.13 (m, 5H, H-naphthalene +H-Ar), 8.48 (s, 1H, H-naphthalene), 9.15 (s, 1H, H-pyrazole). ^{13}C NMR (300 MHz, DMSO-d_6) δ (ppm): 13.63 (CH_3), 61.14 (CH_2), 121.38, 123.93, 124.21, 127.09, 127.73, 128.39. 128.58, 128.97, 129.76, 129.84, 131.82, 132.07, 132.17, 132.37, 134.92, 135.22 and 137.51 (C-Ar), 144.07 (C-pyrazole), 161.19 COOEt), 188.50 (CO). MS *m/z* (%): 403 [M^+-1] (51), 359 [M^+-CH_3CH_2OH] (68). Anal. Calcd. for $C_{23}H_{17}ClN_2O_3$ (404.85): C, 68.24; H, 4.23; N, 6.92. Found: 68.30; H, 4.18; N, 6.93.

2-(4-chlorophenyl)-4-(naphthalen-2-yl)-2,6-dihydro-7H-pyrazolo[3,4-d]pyridazin-7-one 9

To a solution of compound **8e** (10 mmol) in ethanol (10 mL) hydrazine hydrate (10 mmol) was added under reflux for 5h. After the reaction compilation, the solvent was removed by evaporation under reduced pressure to obtain a white solid powder **9**. The separated solid was dried, and recrystallized from EtOH. Yield (80%), mp: > 300° C. IR (KBr,*v*,cm^{-1}): 3079 (NH), 1656 (C=O). ^{1}H-NMR (300 MHz, DMSO-d_6) δ (ppm): 7.15-7.23 (br, 4H, H-Ar), 7.47 (br, 1H, H-naphthalene), 7.65 (br, 2H, H-naphthalene), 8.23 (br, 2H, H-naphthalene), 8.32 (br, 1H, H-naphthalene), 8.50 (s, 1H, H-naphthalene), 9.63 (s, 1H, H-pyrazole), 12.38(s, 1H, NH). ^{13}C NMR (300 MHz, DMSO-d_6) δ (ppm):110.26 (C-pyrazole), 118.50, 120.37, 122.20, 122.35, 125.12, 125.63, 129.65, 131.19, 132.98, 137.86 and 138.96 (C-Ar), 143.05 (C-pyrazole), 155.65 (CON). MS *m/z* (%):372 [M^+] (45). Anal. Calcd for $C_{21}H_{13}ClN_4O$ (372.08): C, 67.66; H, 3.51; N, 15.03. Found: C, 67.71; H, 3.48; N, 15.01.

General procedure for preparation of pyridine derivatives 10, 11

A mixture of enaminone **2** (10 mmol) and the appropriate active methylene reagents, namely; malononitrile and acetylacetone (10 mmol) and ammonium acetate (0.2g) in glacial acetic acid (10 mL) was heated under refluxing temperature. The reaction was followed up by TLC. After compilation of the reaction, the mixture was treated by an ice-cold sodium bicarbonate solution. The resulting solid products, which were converted into the corresponding pyridine derivatives **10** and **11** were recovered by filtering, followed by water wash, drying, and recrystallized from ethanol.

6-(naphthalen-2-yl)-2-oxo-1,2-dihydropyridine-3-carbonitrile 10

Yield (75%); mp: 197-200 °C (EtOH). IR (KBr, *v*, cm^{-1}): 3349 (NH), 2215 (CN), 1548 (C=O). ^{1}H-NMR (300 MHz, DMSO-d_6) δ (ppm): 7.60-7.69 (m, 3H, 2H-naphthalene+H-pyridine), 7.95-8.19 (m, 5H, 4H-naphthalene+H-pyridine), 8.44 (s, 1H, H-naphthalene), 8.55 (s, 1H, NH). ^{13}C NMR (300 MHz, DMSO-d_6) δ (ppm): 107.31(C-pyridine), 117.40 (CN), 122.47, 122.54, 122.99, 132.24, 133.91, 135.71, 142.64, 150.73 and 153.21 C-naphthalene), 161.1 (C-pyridine), 165.19 (CONH). MS *m/z* (%) 246 [M^+] (17%), 245 [M^+-H] (100), 217 [M^+-CN] (15). Anal; Calcd for $C_{16}H_{10}N_2O$ (246.27): C, 78.03; H, 4.09; N, 11.38. Found: C, 78.41; H, 4.18; N, 11.61.

1-(2-methyl-6-(naphthalen-2-yl)pyridin-3-yl)ethan-1-one 11 [30].

Yield (85%); mp: 112-114°C (EtOH). IR (KBr, *v*, cm^{-1}): 1679 (C=O). ^{1}H-NMR (300 MHz, DMSO-d_6) δ (ppm): 2.60 (s, 3H, CH_3), 2.73 (s, 3H, $COCH_3$), 7.54 (dd, 2H, H-naphthalene, *J* = 3.3 Hz), 7.93-8.06 (m, 4H, 2H-naphthalene+2H-pyridine), 8.27 (d, 2H, H-naphthalene, *J* = 8.4 Hz), 8.71 (s, 1H, H-naphthalene). ^{13}C NMR (300 MHz, DMSO-d_6) δ (ppm): 24.90 (CH_3), 29.45 (CH_3CO), 117.66 (C-pyridine), 124.37, 126.60, 126.64, 127.10, 127.60, 128.36, 128.63, 128.93, 130.97, 132.98, 133,55, 135.00, 138.81(C-naphthalene + 2C-pyridine), 156.83, 157.18 (2C•-N-pyridine), 200.32 ($COCH_3$). MS *m/z* (%): 261 [M^+] (58). Anal. Calcd for $C_{18}H_{15}NO$ (261.12): C, 82.73; H, 5.79; N, 5.36. Found: C, 82.78; H, 5.77; N, 5.32.

General procedure for preparation of compounds 12 and 13.

To a solution of enaminone **2** (10 mmol) in glacial acetic acid (10 mL) different heterocyclic amines, namely**,** 3,5-diamino-1,3,4-triazole and/or 2-aminobenzimidazole were added. The mixtures were refluxed for 10 hours, and followed up by TLC. The reaction mixtures were concentrated and allowed to cool at room temperature. The solid precipitates were filtered off, dried and recrystallized from EtOH to afford products **12** and **13**.

7-(naphthalen-2-yl)-[1,2,4]triazolo[1,5-a]pyrimidin-2-amine 12

Yield (65%), mp 192-195 ° C (EtOH). IR (KBr, *v*, cm^{-1}): 3261 (NH_2), 3058 (CH-Ar), 2981 (CH-alph). ^{1}H-NMR (300 MHz, DMSO-d_6) δ (ppm): 4.3 (br s, 2H, NH_2), 7.56-7.68 (m, 3H, 3H-naphthalene), 7.97- 8.09 (m, 3H, H-naphthalene), 8.14 (d, 1H, H-pyrimidine), 8.76 (s, 1H, H- naphthalene), 8.94 (d, 1H, H-pyrimidine). ^{13}C NMR (300 MHz, DMSO-d_6) δ (ppm): 110.14 (CH-pyrimidine), 125.77, 127.06, 127.26, 127.86, 128.31, 128.51, 129.21, 130.58, 132.32 and 134.18 (C-naphthalene), 147.33 (C-pyrimidine), 155.17 (C-triazolopyrimidine), 155.80 (CH-pyrimidine), 156.02 (C-triazole). MS *m/z* (%): 245 [M^+-NH_2] (100). Anal. Calcd. for $C_{15}H_{11}N_5$ (261.27): C, 68.95; H, 4.24; N, 26.80. Found: C, 70.20; H, 4.16; N, 26.65.

4-(naphthalen-2-yl)benzo[4,5]imidazo[1,2-a]pyrimidine 13

Yield (80%), mp 206-210 °C (EtOH). IR (KBr, *ν*, cm^{-1}): 3056 (CH-Ar), 2937 (CH-alph). ^{1}H-NMR (300 MHz, DMSO-d_6) δ (ppm): 7.52-7.71 (m, 4H, 3Ar-H+ 1H- naphthalene), 7.93-8.11 (m, 4H, H-naphthalene), 8.17 (d, 1H, H-pyrimidine), 8.71 (s, 1H, H-naphthalene), 8.85 (d, 1H, H-Ar), 8.95 (d, 1H, H-pyrimidine). ^{13}C NMR (300 MHz, DMSO-d_6) δ (ppm): 113.23 (C-benzene), 115.23 (C-pyrimidine), 119.22, 122.13 (2C-benzene), 124.75, 124.95, 126.11, 126.13, 128.50, 132.23, 133.12, 135.21 and 138.27 (C-naphthalene), 139.24 (C-benzimidazole), 145.33 (C-benzimidazole), 151.37 (C-imidazolopyrimidine), 157.64, 165.22 (2C-pyrimidine). MS (EI, 70 eV) *m/z* (%):295 [M^+] (4). Anal. Calcd. for $C_{20}H_{13}N_3$ (295.35): C, 81.34; H, 4.44; N, 14.23. Found: C, 81.31; H, 4.48; N, 14.22.

3.2 Biological Activity

3.2.1 Determination of Cytotoxicity Concentration 50 (CC_{50}) by Crystal Violet assay:

A modified version of [36] was used to determine the cytotoxicity. In a U-shaped 96-well plate, 180 µl of prepared stock solution of the synthetic compound was added to row 1 from (A1 to H1), resulting in a concentration of (1:10) from the stock of synthetic compound in the first row. Fresh media was then distributed to all wells from rows 2 to 12, and 180 µl to wells in row 1. Columns 2 through 10 were set up for a two-fold serial dilution. Treating the VERO-E6 monolayer sheets at 90% confluency required 50 µl of each dilution, which were then incubated for 72 hours. After fixing for 3 h at room temperature with 10% formaldehyde, the cells were cleaned and stained with crystal violet solution (0.5%) for 15 min. After washing, the cells were allowed to dry. Using absolute methanol to dissolve the stain, the optical density of the 96-well plate was read using an ELISA reader and the cytotoxicity was calculated using the following equation:

Cytotoxicity = (OD of untreated cells − OD of treated cells) / (OD of untreated cells) × 100.

3.2.2 Inhibitory Concentration 50 (IC_{50}) Determination:

2.4×10^{4} Vero-E6 cells were seeded into each well of 96-well tissue culture plates, and the plates were incubated for the entire night at 37 °C in a humidified environment with 5% CO_2. After giving the cell monolayers one wash with 1x PBS, they were exposed to viral adsorption for one hour at room temperature (RT) using hCoV-19/Egypt/NRC-03/2020 (Accession Number on GSAID: EPI_ISL_430820). The test chemicals were added to the cell monolayers in different concentrations using 100µl of DMEM. After being incubated for 72 hours at 37 °C in a 5% CO_2 incubator, the cells were fixed for 30 min. using 100 µl of 4% paraformaldehyde and stained for 15 minutes at room temperature using 0.1% crystal violet in distilled water. After dissolving the crystal violet dye with 180 µl of 100% methanol in each well, the Anthos Zenyth 200rt plate reader (Anthos Labtec Instruments, Heerhugowaard, Netherlands) was used to measure the optical density of the color at 570 to 690 nm [36]. The compound's half-life (IC_{50}) is the amount needed to lessen the viral-induced cytopathic effect (CPE) by 50% in comparison to the virus control. With a few minor adjustments, the protocol was followed as previously described [37, 38].

3.3. DFT studies

The optimized molecular structures of the mentioned compounds (**8b, d)**, and remdesivir) (fig.15) and all the required DFT visualizations [39] were performed using Gaussian-09W and Gauss view-06. The B3LYP functional and the 6-31G(d,p) basis set have been used for all DFT calculations in accordance with previously published methodologies [40]. The procedure's basis set was also used to compose the geometrical parameters, MEP, and FMOs orbitals.

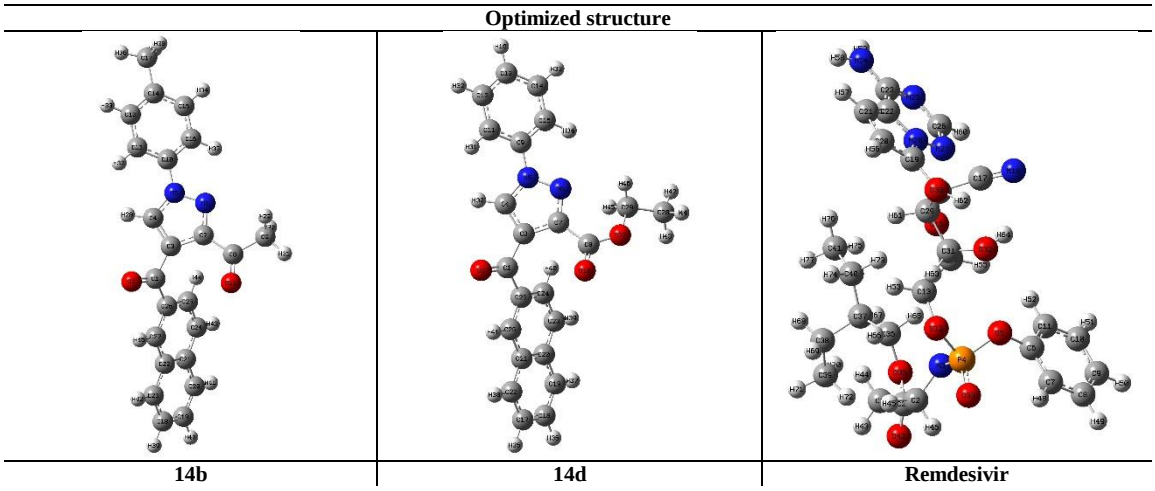

Fig. (15). The optimized structure of compounds 14b,d, and remdesivir. Optimized with DFT-B3LYP/6- 31G(d,p).

3.4. Protein preparation and molecular docking study.

The structures of the compounds were generated using the output of the Gaussian 09 software and saved in the PDB file format. The protein data bank (http://www.rcsb.org.pdb) was used to retrieve the crystal structures of the SARS-CoV-2 spike glycoprotein (PDB ID: 6VSB). We used MOE 2015, a molecular docking program, to carry out the in-silico method. To have the target protein crystal structure ready, we removed NAG molecules and crystal structure subunit A from each 6VSB pdb file, using just subunits B and C. Table 4 showed the molecular docking results of the synthetic derivatives.

3.5. Designing Pharmacophores.

The steps for making pharmacophores, as previously reported [41], are as follows: To begin, the chosen SARS-CoV-2 inhibitors were trained using a flexible alignment dataset in the MOE 2015.10 tool. An example of a flexible alignment output is the alignment score of the configuration (S). Alignments may be better indicated by lower S values. The second step is to transfer the alignment structure with the lowest S value to the MOE window. To use the structures from the alignment training set in a pharmacophore query, use the Pharmacophore Query Editor. After that, the Pharmacophore Search checks the produced model against all the tested compounds (**8a**, **8b**, **8d**, and **8e**). Based on the molecular conformations in the test set database, the application uses the Pharmacophore Preprocessor to generate annotations using the PCH-All (Polarity-Charge-Hydrophobicity) pharmacophore scheme that is currently specified. After that, make some changes to the query and investigate the database using the consensus query approach. Lastly, the program generates rmsd (root of the mean square distance) values that represent the degrees of mapping for a certain molecule to a hypothetical model that has been developed.

4. Conclusion

Various synthetic strategies of heterocyclic compounds have been mentioned in this study to develop new innovative scaffolds as highly effectiveness antiviral drugs. Enaminones were first synthesized, after then, their interactions with different reagents in different conditions were performed to get three series of naphthalene hybrid heterocycles. Molecular docking method was used to study the efficiency of the target derivatives as inhibitors of SAES-CoV-2 spike glycoprotein (PDB ID: 6VSB) where derivatives **8b** and **8d** showed good fitting inside the binding site of the protein molecular surface with low binding energy. Using MEP map, we examined the electron distribution and surface locations of the selected compounds. Models of the pharmacophores were ultimately constructed using nine SARS-CoV-2 inhibitors. The synthesized compounds (**8a**, **8b**, **8d**, and **8e**) were found to have strong inhibitory action against SARS-CoV-2 by 3D pharmacophore virtual screening, demonstrating their potential for future drug development efforts. Lastly, the antiviral screening, molecular docking and pharmacophore studies exhibited two promising naphthalene-coupled pyrazoles **8b** and **8d** as anti-SARS-CoV 2 virus.

5. References

[1] M. Hasoksuz, S. Kilic, F. Sarac " Coronaviruses and SARS-COV-2" Turkish journal of Medical Science, **2020**, 50, 549-556. . https://doi.org/10.3906/sag-2004-127

[2] C.J.E. Metcalf, J. Lessler "Opportunities and challenges in modeling emerging infectious diseases" *Science*, **2017**, 357, 149–152. DOI: 10.1126/science.aam8335

[3] X. Zou, K. Chen, J. Zou, P. Han, J. Hao, Z. Han "Single-cell RNA-seq data analysis on the receptor ACE2 expression reveals the potential risk of different human organs vulnerable to 2019-nCoV infection" *Front. Med.*, **2020**,14(2), 85–192. DOI: 10.1007/s11684-020-0754-0

[4] F. Xiao, M. Tang, X. Zheng, C. Li, J. He, Z. Hong "Evidence for gastrointestinal infection of SARS-CoV-2" *Gastroenterology*. **2020**, 158, 1831–1833. DOI: 10.1053/j.gastro.2020.02.055

[5] C. B. Deng, J. Li, L. Y. Li, F. J. Sun.; "Protective effect of novel substituted nicotine hydrazide analogues against hypoxic brain injury in neonatal rats via inhibition of caspase"; *Bioorganic and Medicinal Chemistry Letters*; **2016**, 26, 3195. https://doi.org/10.1016/j.bmcl.2016.04.031

[6] M. A. Elsayed, K. A. Ali, N. A. Abdel-Hafez, A. M. Mohamed, A. E. Amr, S. F. Mohamed, J. M. Campagne, "N-Phenyl Benzohydrazonoyl Halides as an Excellent Precursor of Nitrile Imines for the Preparation of Heterocyclic Compounds" *Polycyclic Aromatic Compounds*, **2024**, 44(2), 1392-1430. https://doi.org/10.1080/10406638.2023.2186446.

[7] S. Makar, T. Saha and S. K. Singh, " Naphthalene, a versatile platform in medicinal chemistry: Sky-high perspective"Eur. J. Med. Chem., **2019**, 161, 252–276. DOI: 10.1016/j.ejmech.2018.10.018

[8] K. Vogel, J. Sterling, Y. Herzig, A. Nudelman "α-1-Tributyltin-O-2, 3- bisacetyl-4, 6-ethylidene-glucose as a convenient glycosidation reagent: an efficient synthesis of etoposide" *Tetrahedron*, **1996**, 52, 3049-3056. https://doi.org/10.1016/0040-4020(95)01122-6

[9] B. Chopra, A.K. Dhingra, R.P. Kapoor, D.N. Parsad "Synthesis and antimicrobial activity of naphthylamine analogs having azetidinone and thiazolidinone moiety" *Journal of Exploratory Research in Pharmacol*ogy, **2017**, 2(4), 105-112. **https://doi.org**/10.14218/JERP.2017.00005
[10] C.-F. Chang, K.-C. Liao, C.-H. Chen "2-Phenylnaphthalene derivatives inhibit lipopolysaccharide-induced pro-inflammatory mediators by down regulating of MAPK/NF-κB pathways in RAW 264.7 macrophage cells" *PLOS One*, **2017**, 12, 168945. https://doi.org/10.1371/journal.pone.0168945
[11] C.-H. Tseng, C.-K. Lin, Y.-L. Chen, C.-K. Tseng, J.-Y. Lee, J.-C. Lee "Discovery of naphtho [1, 2-d] oxazole derivatives as potential anti HCV agents through inducing heme oxygenase-1 expression" *European Journal of Medicinal Chem*istry, **2018**, 143, 970-982. https://doi.org/10.1016/j.ejmech.2017.12.006
[12] Z. Wang, L. Li, Z. Zhou, Y. Geng, Y. Chen, T. Sun; "Design, synthesis, configuration research, and in vitro antituberculosis activities of two chiral naphthylamine substituted analogs of bedaquiline" *Journal of Heterocyclic Chemistry*, **2017**, 54, 1024-1030. https://doi.org/10.1002/jhet.267
[13]N. Jarari, N. Rao, J.R. Peela, K.A. Ellafi, S. Shakila, A.R. Said, N.K. Nelapalli, Y. Min, K.D. Tun, S.I. Jamallulail "A review on prescribing patterns of antihypertensive drugs" *Journal of Clinical Hypertension*, **2016**, 22 (7). https://doi.org/10.1186/s40885-016-0042-0
[14] N. Kerru, A. Singh-Pillay, P. Awolade, P. Singh "Current anti-diabetic agents and their molecular targets: a review" *European Journal of Medicinal Chem*istry, **2018**, 152, 436-488. https://doi.org/10.1016/j.ejmech.2018.04.061
[15] S. Gomathy, G. Singh, B. Gowramma, A.S. Antony, K. Elango "Synthesis and anti-Parkinson's screening of some novel 2-(naphthalen-1-yl)-N-[2-substituted (4-oxothiazolidin-3-yl)] acetamide derivatives" *Int. J. Health Allied Sci.*, **2012**, 1(4), 244-248. https://doi.org/10.4103/2278-344X.107871

[16] C. Kaiser, J.J. Lafferty "Piperidylidene derivatives of benzo-fused xanthenes, thioxanthenes and dibenzoxepins and antipsychotic use thereof" *Google Patents* (**1978**), US4073912A.
[17] R.V. Shingalapur, K.M. Hosamani, R.S. Keri, M.H. Hugar; "Derivatives of benzimidazole pharmacophore: synthesis, anticonvulsant, antidiabetic and DNA cleavage studies" *European Journal of Medicinal Chem*istry, **2010**, 45(5), 1753-1759. https://doi.org/10.1016/j.ejmech.2010.01.007
[18]J.I. Andrés-Gil, M.J. Alcázar-Vaca, J.M. BartolomeNebreda, F.J. Fernández Gadea , M.H.M. Bakker, A.A.H. Megens "Fused heterocyclic isoxazoline derivatives and their use as anti-depressants" *Google Patents* (**2004**), 2004/018483 & C A 02494557
[19] Ö. SoyluEter , G. N. Duran, M. Özbil, F. Göktaş, G. C. Üstündağ, N. Karalı; "Antiviral activity and molecular modeling studies on 1*H*-indole-2,3-diones carrying a naphthalene moiety"; *Journal of Molecular Structure*, **2023**, 1281, 135100. https://doi.org/10.1016/j.molstruc.2023.135100
[20] V. Giongo, A. Falanga, C. P. P. D. Melo, G. B. D. Silva, R. Bellavita, S. G. D. Simone, I. C. Paixão , S. Galdiero, **"**Antiviral Potential of Naphthoquinones Derivatives Encapsulated within Liposomes**"** *Molecules*, **2021**, 26(21), 6440. https://doi.org/10.3390/molecules26216440
[21] M. Decker, Design of hybrid molecules for drug development, Elsevier, Amsterdam, **2017** ·
[22] K. A. Ali, N. A. Abdel Hafez, M. A. Elsayed, M. M. Elshahawi, S. M. El-Hallouty, A. E. Amr, " screening and molecular docking studies of new heterocycles with trimethoxyphenyl scaffold as combretastatin analogues" *Mini-reviews in medicinal chemistry*, **2018**, 18(8), 717-727. https://doi.org/10.2174/1389557517666170425104241.
[23] K. A. Ali, M. A. Elsayed, A. M. Farag "Synthesis of some new pyridine-2,6-bis-heterocycles" 1913**.** https://doi.org/10.3987/COM-12-12483.
[24] S. F. Mohamed, H. S. Abd-Elghaffar, A. E. Amr, D. H. Elnaggar, E. S. Abou- Amra, H. M. Hosny, A. M. Mohamed, D. N. Abd El-Shafyd. **"**New Poly Heterocyclic Compounds Based on Pyrimidine-2-Thiones: Synthesis, Evaluation of Putative Antiviral Agents, DFT Calculation, and Molecular Modeling", *Journal of Molecular Structure* , **2023**, 1291, 136083. https://doi.org/10.1016/j.molstruc.2023.136083
[25] N. A Alkenzi, W. I. El-Sofany, A. M. Mohamed and W. A. El-Sayed, " Synthesis, Molecular Modeling and Antiviral Activity of Novel Triazole Nucleosides and Their Analogs" *Russian Journal of General Chemistry* , **2019**, 89(9), 1896-1904. https://doi.org/10.1134/S1070363219090263
[26] C.J. Gordon, E. P. Tchesnokov, E. Woolner, J. K. Perry, J. Y. Feng, D. P. Porter, M. Gotte, "Remdesivir is a direct -acting antiviral that inhibits RNA-dependent RNA polymerase from syndrome coronavirus 2 with high potency", *Journal of Biological chemistry*, **2020,** 295(20), 6785-6797. https://doi.org/10.1074/jbc.RA120.013679.
[27] A. M. Mohamed, W. A. El-Sayed, M. A. Alsharari, H. R. M. Al –Qalawi, M. O. Germoush, " Anticancer activities of some Newly Synthesized Pyrazole and Pyrimidine Derivatives", *Archives of Pharmacological Research* , **2013**, 36(9), 1055-1065. https://doi.org/10.1007/s12272-013-0163-x
[28] M. E. Salem, E. M. Mahrous, E. A. Ragab, M. S. Nafie, K. M. Dawood "Synthesis and Anti -Breast Cancer Potency of Mono- and Bis-(pyrazolyl[1,2,4]triazolo[3,4-*b*][1,3,4]thiadiazine) Derivatives as EGFR/CDK-2 Target Inhibitors" *ACS Omega* **2023**, *8* (38), 35359-35369. https://doi.org/ 10.1021/acsomega.3c05309

[29] O. M. Ahmed, M. A. Mohamed, R. R. Ahmed, S. A. Ahmed Synthesis and anti-tumor activities of some new pyridines and pyrazolo[1,5-*a*]pyrimidines. *European Journal of Medicinal Chemistry*, **2009**, 44(9), 3519-3523. https://doi.org/10.1016/j.ejmech.2009.03.042
[30] B. Al-Saleh, M. M. Abdelkhalik, A. M. Eltoukhy, M. H. Elnagdi, ,Enaminones in Heterocyclic Synthesis: a New Regioselective Synthesis of 2,3,6-Trisubstituted Pyridines, 6-Substituted-3 Aroylpyridines and 1,3,5-Triaroylbenzenes, *Journal of heterocyclic chemistry*, **2002**, 39, 1035. https://doi.org/10.1002/jhet.5570390528
[31] K. Fukui, "Role of frontier orbitals in chemical reactions". *science*, **1982**, 218(4574), 747-754. https://www.jstor.org/stable/1689733
[32] R. G. Parr, R. G. Pearson, "Absolute hardness: companion parameter to absolute electronegativity";. *Journal of the American chemical society*, **1983**, 105(26), 7512-7516. https://doi.org/10.1021/ja00364a005
[33] S. Saravanan, V. Balachandran, "Quantum chemical studies, natural bond orbital analysis and thermodynamic function of 2, 5-dichlorophenylisocyanate";. *Spectrochimica Acta Part A: Molecular and Biomolecular Spectroscopy*, **2014**, 120, 351-364. https://doi.org/10.1016/j.saa.2013.10.042.
[34] R. R. Deshpande, A. P. Tiwari, N. Nyayanit, M. Modak, "In silico molecular docking analysis for repurposing therapeutics against multiple proteins from SARS-CoV-2";. *European journal of pharmacology*, **2020**, 886, 173430. https://doi.org/10.1016/j.ejphar.2020.173430
[35] J. S. Mason, A. C. Good, E. J. Martin, "3-D pharmacophores in drug discovery";. *Current pharmaceutical design*, **2001**, 7(7), 567-597. https://doi.org/10.2174/1381612013397843
[36] D. E. Gordon, et al., "A SARS-CoV-2 protein interaction map reveals targets for drug repurposing". *Nature*, **2020**. 583(7816), 459-468. https://doi.org/10.1038/s41586-020-2286-9
[37] M. Scudellari, "How the coronavirus infects cells—and why Delta is so dangerous". *Nature*; **2021**, 595, 640-644. *doi:* https://doi.org/10.1038/d41586-021-02039-y
[38] A. A. T. Naqvi, et al., "Insights into SARS-CoV-2 genome, structure, evolution, pathogenesis and therapies: Structural genomics approach"; *Biochimica et Biophysica Acta (BBA)-Molecular Basis of Disease*, **2020**. 1866(10), 165878. https://doi.org/10.1016/j.bbadis.2020.165878
[39] C. L. Christenholz, D. A. Obenchain, R. A. Peebles, S. A. Peebles, "Rotational spectroscopic studies of C–H⋯ F interactions in the vinyl fluoride⋯ difluoromethane complex";. *The Journal of Physical Chemistry A*, **2014**, 118(9), 1610-1616. https://doi.org/10.1021/jp500312r ·
[40] A. Y. Hassan, S. N. Shabaan, S. A. El-Sebaey, E. S. Abou-Amra, "Synthesis of pyrido-annelated [1, 2, 4, 5] tetrazines,[1, 2, 4] triazepine, and [1, 2, 4, 5] tetrazepines for anticancer, DFT, and molecular docking studies"; *Scientific Reports* **2023**, 13(1), 5585. https://doi.org/10.1038/s41598-023-32421-x
[41] S. A. Ellithy, A. Abdel-Rahman, E. S. Abou-Amra, A. A. Hassan, "Glycosyl Thiourea: Synthesis, Cyclization, Reaction, Molecular Docking, and Evaluation as Potential Acetylcholinesterase Inhibitors"; *Egyptian Journal of Chemistry* **2023**, 66(13), 1759-1777. https://doi.org/10.21608/EJCHEM.2023.244506.8770